

2021-10-30


## CaMKII binds both substrates and activators at the active site [preprint]

Can Ozden  
*University of Massachusetts Amherst*

*Et al.*

### Let us know how access to this document benefits you.

Follow this and additional works at: [https://escholarship.umassmed.edu/faculty\\_pubs](https://escholarship.umassmed.edu/faculty_pubs)

 Part of the [Amino Acids, Peptides, and Proteins Commons](#), [Biochemistry Commons](#), and the [Enzymes and Coenzymes Commons](#)

---

### Repository Citation

Ozden C, Sloutsky R, Mitsugi T, Santos N, Agnello E, Gaubitz C, Foster J, Lapinkas E, Esposito EA, Saneyoshi T, Kelch BA, Garman SC, Hayashi Y, Stratton MM. (2021). CaMKII binds both substrates and activators at the active site [preprint]. University of Massachusetts Medical School Faculty Publications. <https://doi.org/10.1101/2020.10.25.354241>. Retrieved from [https://escholarship.umassmed.edu/faculty\\_pubs/2094](https://escholarship.umassmed.edu/faculty_pubs/2094)

Creative Commons License



This work is licensed under a [Creative Commons Attribution-NonCommercial-No Derivative Works 4.0 License](#). This material is brought to you by eScholarship@UMassChan. It has been accepted for inclusion in University of Massachusetts Medical School Faculty Publications by an authorized administrator of eScholarship@UMassChan. For more information, please contact [Lisa.Palmer@umassmed.edu](mailto:Lisa.Palmer@umassmed.edu).

## 1 CaMKII binds both substrates and activators at the active site

2  
3 Can Özden<sup>1,2</sup>, Roman Sloutsky<sup>1</sup>, Tomohiro Mitsugi<sup>5</sup>, Nicholas Santos<sup>1</sup>, Emily Agnello<sup>1</sup>, Christl  
4 Gaubitz<sup>4</sup>, Joshua Foster<sup>2</sup>, Emily Lapinskas<sup>1</sup>, Edward A. Esposito<sup>3</sup>, Takeo Saneyoshi<sup>5</sup>, Brian A.  
5 Kelch<sup>4</sup>, Scott C. Garman<sup>1</sup>, Yasunori Hayashi<sup>5</sup>, Margaret M. Stratton<sup>1</sup>†  
6

7 <sup>1</sup>Department of Biochemistry and Molecular Biology, University of Massachusetts, Amherst, MA  
8 01003, USA. <sup>2</sup>Molecular and Cellular Biology Graduate Program, University of Massachusetts,  
9 Amherst, MA 01003, USA. <sup>3</sup>Malvern Panalytical, Northampton, MA 01060, <sup>4</sup>Department of  
10 Biochemistry and Molecular Biotechnology, University of Massachusetts Chan Medical School,  
11 Worcester, MA 01605, USA. <sup>5</sup>Department of Pharmacology, Kyoto University Graduate School  
12 of Medicine, Kyoto, Japan.

13  
14 † Corresponding author. Email: mstratton@umass.edu (M.M.S.)  
15  
16

### 17 ABSTRACT

18 Ca<sup>2+</sup>/calmodulin dependent protein kinase II (CaMKII) is a signaling protein that is required for  
19 long-term memory formation. Ca<sup>2+</sup>/CaM activates CaMKII by binding to its regulatory segment,  
20 thereby freeing the substrate binding site. Despite having a large variety of interaction partners,  
21 the specificity of CaMKII interactions have not been structurally well-characterized. One  
22 exceptional feature of this kinase is that interaction with specific binding partners persistently  
23 activates CaMKII. To address the molecular details of this, we solved X-ray crystal structures of  
24 the CaMKII kinase domain bound to four different binding partners that modulate CaMKII activity  
25 in different ways. We show that all four partners bind in the same manner across the substrate  
26 binding site. We generated a sequence alignment based on our structural observations, which  
27 revealed conserved interactions. Using biochemistry and molecular dynamics simulations, we  
28 propose a mechanistic model that persistent CaMKII activity is facilitated by high affinity binding  
29 partners, which compete with the regulatory segment to allow substrate phosphorylation.  
30

### 31 INTRODUCTION

32 Ca<sup>2+</sup>/calmodulin-dependent protein kinase II (CaMKII) is a central signaling protein that controls  
33 various cellular functions such as synaptic plasticity, cytoskeletal regulation, cell growth and  
34 division, gene transcription and ion channel modulation [1]. CaMKII biology has been an active  
35 focus of research especially because of its crucial role in long-term potentiation (LTP), which is  
36 the basis for long-term memory [2, 3]. CaMKII is highly abundant in the forebrain postsynaptic  
37 density (PSD) fraction, where it makes up to 2% of total protein [4]. CaMKII is a multisubunit  
38 complex made up of 12-14 subunits, which is oligomerized by the hub domain (**Fig. 1a**). Each  
39 CaMKII subunit contains a Ser/Thr kinase domain, autoinhibitory/regulatory segment, variable  
40 linker region, and a hub domain (**Fig. 1b**). LTP is governed by many molecular interactions,  
41 including dozens with CaMKII, however the structural details of these interactions are lacking  
42 (**Fig. 1c**) [5].  
43

44 Ca<sup>2+</sup>/calmodulin (Ca<sup>2+</sup>/CaM) activates CaMKII by binding to the regulatory segment and thereby  
45 freeing the substrate binding site. This well-understood mechanism triggers trans-  
46 autophosphorylation of T286, which renders CaMKII constitutively active until T286 is  
47 dephosphorylated. CaMKII has also been shown to maintain activity in the absence of  
48 Ca<sup>2+</sup>/CaM and T286 phosphorylation by another mechanism that invokes two binding partners  
49 [6-9], for which we lack a clear mechanism. There are two binding partners (NMDA receptor and  
50 Tiam1) that have been shown to be activators of CaMKII after the Ca<sup>2+</sup> stimulus dissipates, with

51 or without T286 phosphorylation [7-9]. The GluN2B subunit of the NMDA receptor is a known  
52 substrate of CaMKII [10, 11], and to this point, the best studied CaMKII activator [12].  
53  $\text{Ca}^{2+}$ /CaM-activated CaMKII has been shown to form a persistent complex with GluN2B, which  
54 locks CaMKII in an active conformation, as long as binding persists [7, 11]. To date, persistent  
55 binding of CaMKII to GluN2B and resultant activation has been explained by a hypothetical  
56 model [8]. In this model, GluN2B first binds to  $\text{Ca}^{2+}$ /CaM-activated CaMKII close to the active  
57 site (termed S-site), presenting Ser 1303 for phosphorylation. Then, GluN2B stays persistently  
58 bound at the base of the CaMKII C-lobe, away from the active site (termed T-site), while freeing  
59 the S-site to bind and phosphorylate other substrates. This model has been widely accepted in  
60 the field, but to date, there is no structural data supporting it.

61  
62 Another known activator is Tiam1, a Rac guanine-nucleotide exchange factor (RacGEF), and it  
63 is phosphorylated multiple times by CaMKII. The carboxy tail of Tiam1 also forms a stable  
64 complex with CaMKII using a pseudosubstrate sequence (alanine at the phosphorylation site).  
65 This Tiam1:CaMKII interaction leads to reciprocal activation of Tiam1 and CaMKII in a complex  
66 known as the reciprocally activating kinase-effector complex (RAKEC) [9]. On the other hand,  
67 Densin-180 (LRRC7) is a postsynaptic scaffolding protein. It also forms a stable complex with  
68 CaMKII through a pseudosubstrate sequence (Ile at the phosphorylation site), but unlike  
69 GluN2B or Tiam1, it inhibits kinase activity [13, 14]. Finally, the AMPA receptor subunit GluA1  
70 is a CaMKII substrate but not a known activator [15, 16]. GluA1 phosphorylation by CaMKII is  
71 important for synaptic plasticity [17-19].

72  
73 In the current study, we solved new co-crystal structures of the CaMKII kinase domain bound to  
74 peptides from GluN2B, Tiam1, Densin-180, and GluA1. Using these structures as starting  
75 points, we compared molecular dynamics (MD) simulations of the kinase domain in complex  
76 with GluN2B, Tiam1, and a previously solved structure with CaMKII bound to an inhibitor,  
77 CaMKIIN1 [20]. Combining this structural information and observations obtained from MD  
78 simulations with the biophysical and biochemical measurements has allowed us to clarify  
79 important interactions that drive binding and propose a working model for maintaining CaMKII  
80 activity in the absence of  $\text{Ca}^{2+}$ /CaM.

## 81 82 **RESULTS**

83  
84 The studies outlined below include characterization of peptides from the following five binding  
85 partners: GluN2B (residues 1289-1310), GluA1 (residues 818-837), Densin-180 (residues 797-  
86 818), and Tiam1 (residues 1541-1559). We also include CaMKIIN1 (residues 37-58) in these  
87 studies, which is a known endogenous inhibitor of CaMKII [21-23]. Unless otherwise specified,  
88 all experiments were conducted in the background of an inactivating CaMKII mutation (D135N).

### 89 90 **CaMKII kinase domain interacts similarly with different binding partners**

91 We used a fluorescence polarization (FP) assay to measure binding of the CaMKII kinase  
92 domain to the five peptides listed above. Four out of five peptides bound to the kinase with  
93 similar affinities, where  $K_d$  values ranged from 1.3  $\mu\text{M}$  to 4.5  $\mu\text{M}$  (GluN2B  $K_d = 1.3 \pm 0.05 \mu\text{M}$ ,  
94 CaMKIINtide  $K_d = 2.9 \pm 0.23 \mu\text{M}$ , Densin-180  $K_d = 3.4 \pm 0.22 \mu\text{M}$ , and Tiam1  $K_d = 4.5 \pm 0.43 \mu\text{M}$ )  
95 (**Fig. 2b**). The one exception was GluA1, which bound with a significantly lower affinity ( $K_d =$   
96  $>50 \mu\text{M}$ ) (**Fig. 2b**). FP measurements require the addition of a fluorophore to the peptide as well  
97 as a small amount of detergent to avoid nonspecific interactions with the fluorophore. To obtain  
98 binding energetics in the absence of a fluorophore and detergent, we used isothermal titration  
99 calorimetry (ITC). These measurements also revealed similar affinities across peptides except  
100 for GluA1. The  $K_d$  values calculated from ITC were significantly lower for the tight binders,  
101 ranging from 56 nM – 1.15  $\mu\text{M}$  (GluN2B  $K_d = 128 \pm 18.3 \text{ nM}$  CaMKIIN2  $K_d = 56 \pm 12.5 \text{ nM}$ , Densin-

102 180  $K_d = 666 \pm 91.1$  nM, Tiam1  $K_d = 1.15 \pm 0.09$   $\mu$ M) (**Fig. S2, Table S1**). The reason for the  
103 difference between the two methods is likely that binding is tighter in the absence of detergent  
104 and bulky aromatic groups from the fluorophore. In contrast, GluA1 consistently had a  
105 significantly lower affinity ( $K_d > 66$   $\mu$ M).

106  
107 We solved 13 total crystal structures of the kinase domain of CaMKII with the active site  
108 occupied by a nucleotide ligand or empty and bound to one of four peptides: GluN2B, GluA1,  
109 Densin-180, and Tiam1 (**Fig. 2, S1**). All structures have resolutions within the range of 1.85 -  
110 2.7 Å (**Table 1, 2**).

111  
112 We solved nine structures of the CaMKII kinase domain bound to the GluN2B peptide. The first  
113 two structures are the WT kinase domain bound to WT GluN2B peptide, one with ADP in the  
114 active site (PDB:6XDU) and one with an empty nucleotide binding pocket (PDB:6XDL). The next  
115 two structures are the D135N kinase domain bound to WT GluN2B peptide with either ATP  
116 (PDB:6XBX) or methyl 6-O-(N-heptylcarbamoyl)- $\alpha$ -D-glucopyranoside (hecameg)  
117 (PDB:6XBP) in the nucleotide binding pocket. The other five structures are the D135N kinase  
118 domain bound to the phosphomimetic GluN2B peptide (S1303D). Two of these structures have  
119 ATP bound in the nucleotide binding pocket (PDB:7KL1,6XOE) and two have empty nucleotide  
120 binding pockets (PDB:7KL4,7KL2), all four of these had different unit cell dimensions. The 5<sup>th</sup>  
121 structure has hecameg bound in the nucleotide binding pocket (PDB:7KL0). In all nine  
122 structures, we observed that the interaction between the GluN2B peptide and the kinase domain  
123 is identical.

124  
125 We solved two structures of the kinase domain bound to the Tiam1 peptide, one with ATP in the  
126 nucleotide binding pocket (PDB:6XFO) and one with an empty nucleotide binding pocket (PDB:  
127 6X8V). Finally, we solved structures of the kinase domain bound to the Densin-180 peptide  
128 (PDB:6X5G) and the GluA1 peptide (PDB:6X5Q), both with empty nucleotide binding pockets.

129  
130 Across all 13 structures, we observed that all peptides interacted with the same surface on the  
131 kinase domain. The overall fold of the kinase domain is similar in all structures with a range of  
132 C $\alpha$  RMSD values from 0.583 - 1.611 Å. We resolved 14-19 residues in each peptide (**Fig. 2a,**  
133 **S1**). GluN2B and Densin-180 peptides bound in completely extended conformations across the  
134 substrate binding site. Tiam1 and GluA1 peptides adopted short helical turns, similar to what  
135 was previously observed in the CaMKIINtide structure [20]. Additionally, Densin-180 forms an  
136 intrachain electrostatic interaction between the -3 position arginine and upstream aspartate  
137 (numbering is based on the prototypical GluN2B substrate with the phosphorylation site set to  
138 zero).

139  
140 **Sequence alignment of CaMKII binding partners based on high-resolution structures**

141 So far, predicting CaMKII interaction partners has been difficult due to conformational  
142 heterogeneity in binding. For example, our structures revealed that several peptides have  
143 helical turns, which shifted the register of conserved interactions (Tiam1, GluA1, and the  
144 previously observed CaMKIINtide). We now provide an updated sequence alignment based on  
145 our structural observations (**Fig. 2c**). The two peptides that are substrates (GluN2B and GluA1)  
146 have the phosphosite facing the nucleotide binding pocket, such that both peptides are docked  
147 at the active site, ready to be phosphorylated. The critical residues of the binding partner  
148 mediating this interaction are conserved at positions +1, -2, -3, -5, and -8, as discussed below  
149 (**Fig. 2c**).

150  
151  
152

## 153 **Conserved hydrophobic interactions**

154  
155 Interactions at the +1 position. We observed in our structures that a small hydrophobic residue  
156 is preferred at the +1 position, which has been previously noted [24-28] (**Fig. 2c**). In all  
157 structures, backbone atoms of the +1 position residue hydrogen bonds with the backbone of  
158 G175 (**Fig. 3**). Adjacent to G175, there is a hydrophobic patch formed by F173, P177, L185,  
159 and Y222. GluA1, CaMKIIN, and Densin-180 all have Val or Ile at the +1 position, which are  
160 buried in this hydrophobic groove. In GluN2B and Tiam1, Tyr and Leu, respectively, occupy this  
161 position and face out of the groove. Tyr is too large and polar to favorably interact with the  
162 groove. Leu is the C-terminal residue on the Tiam1 peptide which may be why it does not stably  
163 interact with the groove in the structure, which is discussed further below.

164  
165 We performed MD simulations of the kinase domain in complex with extended versions of  
166 peptides from GluN2B (1263-1328, adding 32 N-terminal residues and 20 C-terminal residues)  
167 and Tiam1 (1513-1581, adding 28 N-terminal residues and 22 C-terminal residues) and the full-  
168 length CaMKIIN1 protein (adding 41 N-terminal residues and 22 C-terminal residues). In these  
169 simulations, extended peptides interact via two residues (+1 and +4 positions in NR2B and  
170 Tiam1, +1 and +2 in CaMKIINtide; **Fig. S3f-h**) with the hydrophobic patch formed by F173,  
171 P177, L185, and Y222. The +1 leucine and +4 isoleucine of Tiam1 pack with the four kinase  
172 residues into a stable conformation, with pairwise RMSD of less than 2 Å – meaning that  
173 between any two frames in the simulation, the RMSD of these atoms is lower than 2 Å (**Fig.**  
174 **S3f**). The interaction is more fluid for GluN2B and CaMKIIN1, but their respective residues  
175 remain in close proximity to the patch throughout the trajectory (**Fig S3g, h**).

176  
177 Hydrophobic interaction at the -5 position. All CaMKII interactors studied here have a conserved  
178 leucine residue at the -5 position, which fits into a hydrophobic pocket on the kinase domain  
179 comprised of F98, I101, V102, and I205 (**Fig. 3, 4a**). In our structures, leucine is 3.3-4.5 Å from  
180 the four hydrophobic residues, indicating a tight interaction. In the CaMKIINtide structure, a turn  
181 motif is facilitated by two glycine residues, which orients the leucine into this pocket [20]. In  
182 simulations of GluN2B, Tiam1, and CaMKIINtide, this interaction also demonstrates high  
183 structural integrity, with pairwise RMSD below 2 Å (**Fig. 4b**).

184  
185 Docking site mediated by W214. In both Densin-180 and CaMKIINtide structures, the  
186 sidechains of proline and isoleucine (highlighted blue in **Fig. 2c**) pack against W214 on the  
187 kinase domain (**Fig. 4c**). Additionally, for Densin-180, the guanidino group of R808 at the -7  
188 position hydrogen bonds with the backbone carbonyl group of W214 and the sidechain of Q224.  
189 In simulations of CaMKIIN1, W214 and Q224 interact persistently, with pairwise RMSD below  
190 1.5 Å (**Fig. 4e**). In the simulation of Tiam1 bound to the kinase domain, the leucine at position  
191 -14 moves to form a persistent interaction with W214 (**Fig. 4c, e**, highlighted blue in **Fig. 2c**).  
192 However, in the Tiam1 crystal structure, this leucine is close to the N-terminus, which interacts  
193 with another monomer in the asymmetric unit, pulling the leucine >13 Å from W214 in one  
194 monomer, and it is not resolved in the other monomer.

195  
196 We used FP to measure the effect on peptide binding to a kinase domain harboring a mutation  
197 at this tryptophan (W214A). The W214A mutation complete abolished CaMKIINtide binding,  
198 whereas the effects on the other binding partners were not as severe (2- to 4-fold decreased  
199 affinity) (**Fig. 4d, S3a, b, c**). Although both CaMKIINtide and Densin-180 structures show an  
200 interaction with W214, mutation at this site dramatically decreased CaMKIINtide binding  
201 completely but only had a marginal effect on Densin-180 binding (**Fig. 4d**). CaMKIINtide  
202 docking onto W214 likely stabilizes its helical motif, which properly orients the -5 leucine into the  
203 hydrophobic pocket. When W214 is mutated, this interaction is disrupted and the -5 leucine

204 interaction is unlikely to be maintained in CaMKIINtide, completely disrupting binding. Densin-  
205 180 does not have a helical motif, which may explain why the W214A mutant does not have a  
206 drastic effect.

207

## 208 **Electrostatic interactions provide specificity**

209

210 Ionic interactions at the -2 position. Glutamine is commonly at the -2 position of CaMKII  
211 interactors [24-26, 28]. Indeed, all four peptides in our structures have glutamine at -2, allowing  
212 us to resolve the important interactions mediated by both the backbone and the sidechain at this  
213 position (**Fig. 3**). The -2 glutamine sidechain amide oxygen forms a hydrogen bond with the  
214 backbone of G178, and the amino group interacts with the sidechain of Y179. The backbone  
215 carbonyl interacts with sidechain of K137, and the backbone amino group interacts with E139,  
216 which has also been shown to be important for binding (**Fig. S4, S4j**) [8]. Of note, CaMKIINtide  
217 has a serine at the -2 position instead of glutamine (**Fig. 2c**). In this structure, the serine  
218 sidechain is flipped relative to glutamine, which enables hydrogen bonding with E139 and K137  
219 sidechains [20]. This observation is consistent with a previous study, which showed that  
220 CaMKIINtide binding to CaMKII was reduced when this serine was mutated to alanine [29].

221

222 Conserved salt bridge close to the active site. The -3 position is a conserved basic residue,  
223 arginine or lysine, which interacts with conserved glutamate residues on the kinase domain [20,  
224 30]. In the crystal structures, all interactors except for low-affinity binder GluA1 have a basic  
225 residue at the -3 position, which forms salt bridges with two glutamic acid residues (E96, E99)  
226 located on the  $\alpha$ D helix of the kinase domain (**Fig. 3, 5a**). The basic residues of interaction  
227 partners are positioned 2.4 – 4.2 Å between E96 and E99. In the Densin-180 and CaMKIINtide  
228 structures, the -3 arginine is closer to E96, whereas in the Tiam1 structure, the -3 lysine is  
229 closer to E99. In the structures of GluN2B, the -3 position is either more closely associated with  
230 E96 (PDB:6XDL, WT kinase with empty active site; PDB:6XDU, WT kinase with ADP bound) or  
231 E99 (PDB:6XBP, D135N kinase with a detergent bound; PDB:6XBX, D135N kinase with ATP  
232 bound) (**Fig. S4a**). Additionally, in structures where ATP/Mg is also bound (GluN2B, Tiam1), the  
233 side chain of E96 interacts with the hydroxyl group of ribose in the ATP molecule (3.7 – 4.3 Å;  
234 **Fig. S4d**) [31]. These salt bridges are not formed in the GluA1 interaction, because there is a  
235 proline at the -3 position (**Fig. 2c**). In the GluA1 structure, the sidechain of E96 is flipped away  
236 from the peptide compared to the other four structures where it is oriented toward the binding  
237 partner (**Fig. 5a**, inset). Additionally, the sidechain of E99 is not as well-resolved in the GluA1  
238 structure.

239

240 We hypothesized that the reason for GluA1's lower affinity compared to other interaction  
241 partners is due to the lack of this salt bridge. To test this, we created charge reversal mutations  
242 (E→K), and also E→Q mutations that maintain the possibility of hydrogen bonding, but not the  
243 electrostatic component. We directly compared binding affinities of GluN2B (which has a basic  
244 residue at the -3 position) to GluA1 which is lacking this interaction. Single E96K and E99K  
245 mutations were more disruptive to GluN2B binding (affinity decreased 7- and 5-fold,  
246 respectively) compared to GluA1 binding (affinity decreased <2-fold) (**Fig. 5b, c**). The double  
247 lysine mutation (E96/99K) significantly reduced the binding affinity for GluN2B peptide 52-fold  
248 ( $K_d = 68.7 \pm 33.7 \mu\text{M}$ ), while the affinity for GluA1 was roughly the same. In contrast, the E→Q  
249 mutations were less disruptive to binding. GluN2B binding to E96Q and E99Q was only  
250 marginally impaired (affinity decreased <2-fold), while the binding affinity of GluN2B for the  
251 double mutant E96/99Q was weakened by ~4-fold ( $K_d = 5 \pm 0.31 \mu\text{M}$ ) (**Fig. S4b**). All glutamine  
252 mutants showed similar binding to GluA1 compared to WT, where the binding affinities were  
253 >73  $\mu\text{M}$  (**Fig. S4c**). The double glutamine mutant (E96/99Q) expressed more poorly than WT,

254 but the double lysine mutant (E96/99K) reduced the protein expression significantly, likely due  
255 to destabilization.

256  
257 In simulations, the -3 residue also forms a persistent interaction with E139. The -3 arginine of  
258 GluN2B forms 2-4 ionic interactions nearly 100% of the time, mostly with E96 and E139 (**Fig.**  
259 **S4g**), while the lysine of Tiam1 forms 1-2 ionic interactions ~70% of the time, mostly with E139  
260 (**Fig. S4h**). There are no observed interactions between the ATP phosphate groups and the  
261 GluN2B and Tiam1 chains. The interactions observed in the CaMKIIN1 trajectories were very  
262 different. The arginine at the -3 position mostly interacts with E139, minimally with E96, and not  
263 at all with E99 (**Fig. S4i**). The arginine residues at the 0 and -3 positions form very stable  
264 contacts with the ATP phosphates, which locks the ATP in an altered position (**Fig. S4e, j**). This  
265 conformational change precludes the ATP adenosine from forming ionic interactions with the  
266 backbones of D90 and V92, as observed in the crystal structure. As a result, the ATP adenosine  
267 group exits the binding pocket in the CaMKIIN1 trajectories (**Fig. S4e**). In these trajectories, the  
268 serine at the -2 position of CaMKIINtide forms a hydrogen bond with E139 ~98% of the time  
269 (**Fig. S4j**), whereas in GluN2B and Tiam1 trajectories, the glutamine at the -2 position does not  
270 form stable interactions.

271  
272 We performed FP measurements comparing binding of CaMKIINtide to the kinase domain with  
273 charge reversal mutations (E96K, E99K), with and without ATP (**Fig. S4f**). In the absence of  
274 ATP, E96K and E99K both have a ~9-fold reduced binding affinity to CaMKIINtide. MD  
275 trajectories would predict that CaMKIIN1 binding is facilitated by E96 in the presence of ATP,  
276 whereas E99 plays essentially no role. Consistent with this, ATP binding restored E99K binding  
277 to that of WT (D135N), whereas the affinity of E96K was still weakened.

278  
279 Salt bridge at the base of the C-lobe. We observed a conserved basic residue at the -8 position  
280 (arginine or lysine) mediating a salt bridge with E236 on the kinase domain (**Fig. 2c, 3, 6a**). This  
281 likely has not been fully characterized because this position is quite far from the phosphorylation  
282 site (~30 Å), and substrate alignments have not been accurate enough to highlight the  
283 conservation at this position. We tested the effect of mutating E236 to lysine (E236K) on binding  
284 affinity using FP. The E236K mutation completely abolished Tiam1 and GluA1 binding (**Fig. 6b,**  
285 **S5b**). For Densin-180 and GluN2B, E236K binding affinity was reduced ~6-fold ( $K_d = 21 \pm 2.01$   
286  $\mu\text{M}$ ) and ~7-fold ( $K_d = 9.1 \pm 1.27 \mu\text{M}$ ), respectively (**Fig. S5a, S5c**) [8].

287  
288 We investigated whether peptide phosphorylation influences binding affinity by measuring the  
289 affinity of D135N and D135N/E236K to the GluN2B peptide harboring a phosphomimetic  
290 substitution (S→D at position 0). There was very little effect on the phosphomimetic GluN2B  
291 binding to D135N ( $K_d = 2.1 \pm 0.07 \mu\text{M}$ ), whereas affinity for the E236K mutant was reduced ~14-  
292 fold ( $K_d = 28 \pm 13 \mu\text{M}$ ) (**Fig. S5d**). For CaMKIINtide, binding affinity was drastically reduced in our  
293 FP measurement (**Fig. S5e**). However, we performed an ITC experiment using full length  
294 CaMKIIN2 and observed a tight binding constant ( $K_d = 951 \pm 160 \text{ nM}$ ) (**Fig. S2f**). Since we  
295 observed a dramatic difference (~50-fold) between FP and ITC data in D135N CaMKII binding  
296 measurements, it is possible that the detergent is more detrimental to CaMKIIN2 binding  
297 compared to other interactions. This, as well as the favorable entropic term from our ITC  
298 measurements (**Table S1**), is in line with our observation of multiple hydrophobic interactions  
299 being important for this very tight binding inhibitor. A previous study tested the inhibitor efficacy  
300 of CaMKIINtide by doing alanine scanning. When the Arg that interacts with E236 in the crystal  
301 structure was mutated, the interaction was not fully disrupted and CaMKII gained ~10% activity  
302 back [29].

303

304 We investigated the role of E236 in the MD trajectories, which revealed an additional interaction.  
305 In addition to interacting with the -8 position, E236 also forms a persistent hydrogen bond with  
306 the hydroxyl group of Y210, thereby locking the Y210 side chain into a persistent interaction  
307 with W237 with very high structural integrity (RMSD <0.75 Å) (**Fig. S5f, j-l**). We performed  
308 simulations of GluN2B and Tiam1 complexes with an E236K mutation, which showed that the  
309 interaction between Y210 and W237 is disrupted by the loss of the hydrogen bond with Y210  
310 (**Fig. S5k, l**). The resulting movements of the Y210 side chain disrupt the W214 interaction with  
311 Tiam1, which may explain the loss of binding. In GluN2B, the interaction between Y210 and  
312 W237 is also disrupted, but the -8 arginine of GluN2B switches to a highly persistent interaction  
313 with D231.

314

### 315 **Interrogating CaMKII interactions with full-length binding partners**

316 We used a pull-down assay to assess the effect of CaMKII mutations on interactions with full-  
317 length binding partners. We co-transfected HEK293 cells with FLAG-tagged CaMKII $\alpha$  and either  
318 full-length Tiam1, GluN2B, or GFP-CaMKIIN2. Binding was assessed by western blot following  
319 immunoprecipitation with an anti-FLAG antibody. Immunoprecipitation with E236K showed a  
320 remarkable loss of binding for both Tiam1 and GluN2B, similar to our FP data (**Fig. 6d, S6a**).  
321 E236K CaMKII resulted in better binding to CaMKIIN2 compared to WT CaMKII in HEK293 cells  
322 (**Fig S6b**). Our ITC results showed tight binding between E236K CaMKII kinase domain and  
323 CaMKIIN2, and it is known that the E236K mutation disrupts the regulatory segment from  
324 binding [30], thereby facilitating more CaMKIIN binding to E236K compared to WT since the  
325 binding site is more available.

326

327 The immunoprecipitation experiments corroborate our peptide binding data that show the  
328 importance of hydrophobic interactions. Indeed, mutating the hydrophobic pocket at the -5  
329 position (I205K) showed significant loss of CaMKII binding to Tiam1, GluN2B, and CaMKIIN2  
330 (**Fig. 6d, S6**). Finally, the W214A mutation also disrupted binding to Tiam1, GluN2B, and  
331 CaMKIIN2. Consistent with our FP data, CaMKIIN2 binding to W214A is nearly abolished (**Fig.**  
332 **S6b**). We observed a subtle effect on W214A binding the peptide of Tiam1 in our FP assay,  
333 however using full-length Tiam1 in the pull-down revealed a significant effect on binding with  
334 less than 25% relative binding compared to WT (**Fig. 6d, e**). This reflects what we observed in  
335 the simulation using the longer Tiam1 peptide (**Fig. 4c**). Finally, the W214A mutation weakened  
336 the interaction with full-length GluN2B by ~40%, similar to what we observed in our FP  
337 measurements (**Fig S6a**).

338

### 339 **Testing the 2-site binding model**

340 We wanted to directly test the idea of the 2-site binding model (S- and T-sites) [8]. Previous  
341 studies have shown that GluN2B peptide could not be competed off by Syntide-2 even at  
342 millimolar concentrations, which we also observed (**Fig. 6c**) [11]. As noted by Colbran and  
343 colleagues [11], a sequence alignment of Syntide-2 and other substrates reveals that the  
344 Syntide-2 peptide is shorter and therefore missing the -8 position basic residue we discuss  
345 above (**Fig. 6c**). To test whether this is the reason Syntide-2 could not compete GluN2B, we  
346 created an extended version of Syntide-2 by adding three residues to the N-terminus, mimicking  
347 Densin-180. The extended version of Syntide-2 did compete off GluN2B ( $K_i \sim 78 \pm 13.6 \mu\text{M}$ ) (**Fig.**  
348 **6c**). This result shows that Syntide-2 and GluN2B do occupy the same binding site, indicating  
349 that there are not two separate binding sites on the kinase domain.

350

351 If there are not two binding sites, how is CaMKII activity maintained by specific binding partners  
352 like GluN2B? The mode of activation must invoke the phosphorylated form of GluN2B since this  
353 is observed under activating conditions. In a canonical kinase reaction, the kinase first binds  
354 substrate, then transphosphorylation occurs, and finally the substrate is released. We measured



355 the affinity of a phosphomimetic version of GluN2B (S1303D) and observed only a 7-fold  
356 reduction in affinity ( $K_d = 919 \pm 100$  nM) compared to unphosphorylated GluN2B ( $K_d = 128 \pm 18.3$   
357 nM) (**Fig. S2a, g**). We were also able to crystallize the kinase domain bound to GluN2B  
358 S1303D (Table 1), which showed a very similar conformation to WT GluN2B. We hypothesized  
359 that phospho-GluN2B would act as a competitive inhibitor with Syntide-2. We performed  
360 coupled-kinase assays using Syntide-2 as a substrate in the presence of saturating GluN2B  
361 S1303D. As a control, we also measured activity against Syntide-2 in the presence of the  
362 CaMKIIN2 inhibitor. Indeed, high levels of CaMKIIN2 inhibit Syntide-2 phosphorylation, whereas  
363 GluN2B acts as a competitive inhibitor, exemplified by comparable  $V_{max}$  values but an increased  
364  $K_m$  value (**Fig. 7a**).

### 366 **Generalizing CaMKII binding partners**

367 We mined the curated database of CaMKII phosphorylation sites ( $n=418$ ) for consistencies with  
368 our updated alignment and found additional similarities (**Fig. S7**, [www.phosphosite.org](http://www.phosphosite.org)).  
369 Hydrophobic residues (I, V, L, M, F) are found at +1, Q is found at -2, and R is overwhelmingly  
370 found at -3, but also at -2 and -4. Smaller hydrophobic residues (L, V, I or M) are found at -5 and  
371 -6. Generally, the minus direction disfavors P, D, and E. In contrast, acidic residues D and E are  
372 highly favored at +2. GluN2B has D at the +2 position, and we note an interaction with K56 in  
373 several structures, which was also observed in the dEAG-bound structure (PDB: 5H9B) (**Fig.**  
374 **2C**). In addition, S, which may serve as a second phosphorylation site, is strongly disfavored at  
375 nearly every position [28].

### 377 **DISCUSSION**

378 CaMKII has a broad range of substrates and interaction partners. CaMKII recognizes a  
379 consensus sequence R-X-X-S/T, yet the structural details driving these interactions had not  
380 been elucidated. We addressed this by solving co-crystal structures of four binding partners  
381 bound to the CaMKII kinase domain, which allowed us to highlight the interactions mediating  
382 binding. Like many kinases, CaMKII prefers a basic residue at the -3 position [32]. Our crystal  
383 structures, along with others [20, 31], show an electrostatic interaction between the -3 position  
384 and E96/E99. E96 is well-conserved across kinases and known to be important for ATP binding  
385 (**Fig. S7a, S4d**) [31]. E99 is not as well-conserved, even across other CaM-kinases, indicating  
386 that it is not as crucial for ATP binding (**Fig. S7a, c, d**) [33]. Our MD simulations showed E139  
387 interacting with the -3 position (**Fig. S4g-j**). Previous studies have shown that mutations at E139  
388 have a negative effect on AC-2 and GluN2B binding [8, 30]. The simulations also show the 0  
389 and -3 positions of CaMKIIN1 (both Arg) strongly interact with ATP. Further efforts will  
390 interrogate the role of ATP coordination in CaMKIINtide inhibition. The biological ramifications of  
391 the weak interaction between CaMKII and GluA1 will need to be further investigated – where  
392 localization of CaMKII to this receptor by another factor or avidity effects of holoenzyme  
393 localization may be driving GluA1 phosphorylation *in vivo* [37]. Our observation might explain  
394 the molecular basis of a recent study that reported lower levels of S831 phosphorylation in the  
395 hippocampus [38].

397 Upon CaMKII activation, the  $\alpha$ D helix reorients outward, exposing a hydrophobic pocket for  
398 substrate binding, which we observed in all our structures at the -5 position. Kuriyan and  
399 colleagues first identified this hydrophobic pocket as ‘docking site B’, which is comprised of  
400 residues F98, I101, V102, and I205 [20]. Previously, F98 has been reported as part of the ‘S-  
401 site’ and I205 has been reported as part of the ‘T-site’ [8, 30]. However, it is clear from  
402 structures that these residues comprise the same binding site (**Fig. 3, 4a**). This hydrophobic  
403 pocket is highly conserved across CaM-kinases, but not other kinases (**Fig. S7a**). If we compare  
404 structures of a kinase domain with an empty substrate binding site (PDB:6VZK) to a kinase  
405 domain bound to a substrate, it is clear that F98 and V102 undergo a conformational change in

406 the bound state to form the pocket (**Fig. S3d**). This indicates that these hydrophobic residues  
407 shift to accommodate substrate binding, which is likely a large contribution to an observed gain  
408 in kinase domain stability upon each binding (**Fig. S3e**), similar to what we have previously  
409 observed with regulatory segment binding, which is mediated by L290 in the regulatory segment  
410 [34].

411  
412 In all crystal structures, we observed a salt bridge at E236 mediated by a basic residue at the -8  
413 position. Similarly, in the crystal structure of the fly kinase domain bound to a dEAG peptide,  
414 there is a glutamine residue interacting with E236 [28]. In our pull-down assays, a significant  
415 loss of binding was observed for both Tiam1 and GluN2B (**Fig. 6d, S6a**). In the trajectory of  
416 E236K:GluN2B, the -8 arginine switches to interacting with D231, suggesting that this  
417 interaction may compensate for the E236K mutation. E236K is also unable to form the H-bond  
418 with Y210, making the tyrosine side chain more mobile in MD simulations, and disrupting the  
419 interaction between Tiam1 and W214. More work needs to be done to determine whether this  
420 electrostatic interaction provides specificity, which could be exploited in biological experiments.

421  
422 Here, we propose a new mechanistic model for prolonged CaMKII activity in the presence of  
423 specific binding partners. Let's consider the mode of activation by GluN2B as the activator  
424 shown in **Figure 7b**. Phospho-GluN2B is a high affinity binder, and we hypothesize there is an  
425 intermediate step between product dissociation (Rxn 4) and regulatory segment re-binding (Rxn  
426 5). As described, a conformational change is required for regulatory segment re-binding [34],  
427 which would allow substrate phosphorylation if the concentration were high enough (Rxn 7). In  
428 conditions where the activator concentration is high, activator rebinding will be favorable since  
429 this high affinity binder will have a relatively high on-rate and low off-rate. A submicromolar  
430 affinity for a kinase interaction partner/substrate is unique, as typically these interactions are in  
431 the  $K_d$  range of 200  $\mu$ M [35]. GluN2B has the phosphorylatable serine (S1303) which is  
432 potentially a key regulator for this tight interaction as the phosphorylated version would typically  
433 have lower affinity, however in this case it is still sub-micromolar. Indeed, Colbran and  
434 colleagues has been shown that S1303A mutation renders GluN2B an inhibitor, indicating a  
435 very slow off-rate [36]. Tiam1 also allows maintenance of CaMKII activity and binds with low  
436 micromolar affinity, however, Tiam1 does not have a phosphorylatable residue. Perhaps these  
437 high affinity interactors allow these interaction partners to kinetically compete with the regulatory  
438 segment rebinding, yet they allow the enzyme to bind and phosphorylate other substrates. On  
439 the other hand, CaMKIIN binds with nanomolar affinity, which is what makes it a terminal  
440 inhibitor for CaMKII.

441  
442 The crystal structures presented here provide clarity on the interactions between CaMKII and its  
443 binding partners, which will be crucial in guiding biological experiments to assess the  
444 downstream effects of specific interactions. These observations will be crucial in guiding further  
445 experiments, which will necessarily invoke the complexities of the CaMKII holoenzyme  
446 structure. It is intriguing to consider other enzymes that might be modulated in a similar way by  
447 high affinity binding partners as a novel mechanism for prolonged activation.

448  
449  
450  
451  
452  
453  
454  
455  
456

## 457 MATERIALS AND METHODS

458

### 459 Cloning

460 All CaMKII $\alpha$  variants were expressed with an N-terminal His-SUMO tag in a pET vector. All  
461 point mutations were created using site-directed mutagenesis.

462

### 463 Protein Expression and Purification

464 WT CaMKII $\alpha$  kinase domain (residues 7-274) was co-expressed with  $\lambda$  phosphatase in *E. coli*  
465 BL21(DE3). Inactive constructs (D135N) and CaMKIIN2 (*Rattus norvegicus*) were expressed  
466 without  $\lambda$  phosphatase. The cells were induced at 18 °C with 1 mM Isopropyl  $\beta$ -d-1-  
467 thiogalactopyranoside (IPTG) and grown overnight. Following to ~16 hours incubation, cell  
468 pellets were resuspended in Buffer A (25 mM Tris, pH 8.5, 50 mM KCl, 40 mM imidazole, 10%  
469 glycerol) and commercially available protease inhibitors (0.5 mM Benzamidine, 0.2 mM AEBSF,  
470 0.1 mg/mL trypsin inhibitor, 0.005 mM Leupeptin, 1  $\mu$ g/mL Pepstatin), 1  $\mu$ g/mL DNase/50 mM  
471 MgCl<sub>2</sub> were added, then lysed. All following purification steps were performed using an ÄKTA  
472 pure chromatography system at 4 °C. Filtered cell lysate was loaded onto a 5 mL His Trap FF  
473 NiNTA Sepharose column (GE), and eluted with 50% Buffer B (25 mM Tris-HCl pH 8.5, 150 mM  
474 KCl, 1 M imidazole, 10% glycerol). The protein was desalted from excess imidazole using a  
475 HiPrep 26/10 Desalting column using Buffer C (25 mM Tris-HCl pH 8.5, 40 mM KCl, 40 mM  
476 imidazole, 2 mM TCEP, 10% glycerol). His SUMO tags were cleaved with Ulp1 protease  
477 overnight at 4 °C. Cleaved His SUMO tags were separated by a subtractive NiNTA step prior to  
478 an anion exchange step. Proteins were eluted from HiTrap Q-FF with a KCl gradient. Eluted  
479 proteins were concentrated and further purified in gel filtration buffer (25 mM Tris-HCl pH 8.0,  
480 150 mM KCl, 1 mM TCEP, 10% glycerol) using Superdex 75 10/300 GL size exclusion column.  
481 Fractions (>95% purity) were pooled, concentrated, aliquoted and flash frozen in liquid nitrogen,  
482 and stored at -80 °C until needed.

483

### 484 Peptide synthesis

485 Peptides used for co-crystallization were synthesized and amidated at the C-terminus  
486 (Genscript, RIKEN Research Resource Center). Peptides used for fluorescence polarization  
487 assays were synthesized with an additional N-terminal 5-FAM.

488

489 Full length peptide sequences are as follows:

490 Human GLUA1 (residues 818-837): SKRMKGFCLIPQQSINEAIR [Numbering for GluA1 is for  
491 mature peptide, excluding 18 amino acid long signal peptide, following convention in the field.]

492 Human GluN2B (residues 1289-1310): KAQKKNRNKLRQHSYDTFVDL

493 Human GluN2B(S1303D) (residues 1289-1310): KAQKKNRNKLRQHDYDTFVDL

494 Human Densin-180 (residues 797-818): SKSRSTSSHGRRPLIRQDRIVG

495 Mouse Tiam1 (residues 1541-1559): RTLDASHSRMTQLKKQAAL

496

497 Full length peptide sequences for fluorescence polarization assays are as follows:

498 Human GluA1 (residues 813-837): KSRSESKRMKGFCLIPQQSINEAIR

499 Human GluN2B (residues 1289-1310): KAQKKNRNKLRQHSYDTFVDL

500 Human GluN2B(S1303D) (residues 1289-1310): KAQKKNRNKLRQHDYDTFVDL

501 Human Densin-180 (797-818): SKSRSTSSHGRRPLIRQDRIVG

502 Human CaMK2N1 (residues 37-58): GAGQNKRPPLGQIGRSKRVI

503 Mouse Tiam1 (residues 1541-1559): RTLDASHSRMTQLKKQAAL

504 Extended Syntide-2: GRRPLARTLSVAGLPGKK

505

506

507

## 508 **Crystallization and X-Ray Data Collection**

509 Initial crystallization screening was done using the sitting vapor diffusion method at 4°C with  
510 commercially available screening kits. Initial hits were optimized by the hanging vapor diffusion  
511 method if needed. Conditions yielded the crystal formation were included in Table S1, S2. The  
512 ligand-to-protein ratio was kept at 3:1 throughout the co-crystallization attempts. Diffraction data  
513 were collected from crystals flash-frozen in liquid nitrogen at a wavelength of 1.5418 Å using a  
514 Rigaku MicroMax-007 HF X-ray source, which was coupled to a Rigaku VariMax HF optic  
515 system (UMass Amherst). The X-ray data was collected at 100 K.

516

## 517 **Data Processing and Structure Determination**

518 Data sets were integrated, merged, and scaled using HKL-2000. The structures were solved by  
519 molecular replacement (MR) with Phaser using the coordinates of CaMKII $\alpha$  kinase domain  
520 (PDB ID: 6VZK, 100% amino acid sequence identity) as a search model [39]. Peptides were  
521 built into electron density using Coot and refinement was performed with REFMAC5 [40, 41].

522

## 523 **Fluorescence polarization assays**

524 Fluorescent polarization measurements were executed by adding 10  $\mu$ L of 120 nM fluorescein-  
525 labeled peptides (dissolved in 25 mM Tris pH 7.5, 150 mM KCl, 0.02% Tween, 0.02% Triton) to  
526 10  $\mu$ L of mutant CaMKII kinase domains at varying concentrations (25 mM Tris pH 7.5, 150 mM  
527 KCl, 1 mM TCEP, 10% glycerol) in Corning low volume 384-well black flat bottom 384-well  
528 plates. The concentration of ATP and MgCl<sub>2</sub> in peptide stock solution were adjusted to 500  $\mu$ M  
529 and 10 mM, respectively. The competition assay was conducted by mixing 10  $\mu$ L of 2  $\mu$ M  
530 CaMKII kinase domain with 120 nM fluorescein-labeled GluN2B peptide with 10  $\mu$ L of unlabeled  
531 peptides at varying concentrations. The fluorescence polarization was measured using a  
532 Synergy H1 hybrid plate reader (Biotek) with a filter of 485/20 nm excitation and 528/20 nm  
533 emission. Data then was normalized by subtracting the background value ([protein] is zero)  
534 from all data points and each value in the datasets was divided by the difference between the  
535 highest concentration and zero concentration. All data were normalized to the corresponding  
536 wild type measurement where the WT maximum FP value is set to 1. Data were fit using One  
537 site- Specific binding with Hill slope in GraphPad PRISM version 6.01 after subtracting the  
538 background value from individual values.

539

## 540 **Isothermal titration calorimetry**

541 ITC data were obtained using a MicroCal PEAQ-ITC automated calorimeter (Malvern  
542 Panalytical, Westborough, MA). Before each titration, interaction partners were dissolved in gel  
543 filtration buffer and final buffer conditions of CaMKII kinase domain and interaction partners  
544 were matched. GluN2B peptides and CaMKIIN2 protein contain a single tyrosine residue, which  
545 enabled accurate concentration determination. The other peptides lack aromatic residues, and  
546 these required crude weight to estimate concentration. Titrations were performed with different  
547 peptides as titrant into the cell containing D135N or other mutant CaMKII kinase domains  
548 (concentrations are indicated in Table 3). All titrations were performed using the standard 19  
549 injection method, modified to run at 20 °C. The standard 19 injection method in the PEAQ ITC  
550 automated control software (v1.40) is one injection of 0.4  $\mu$ L followed by 18 2  $\mu$ L injections with  
551 a spacing between injections of 150s, a stir speed of 750 rpm, and the reference power set to  
552 10. Data were analyzed using PEAQ ITC analysis software (v1.40) using the one-site fitting  
553 model, and to eliminate integration of some baseline noise, some integration markers were set  
554 manually to obtain better fit.

555

## 556 **Differential scanning calorimetry**

557 Except where noted, all protein samples were diluted to 0.5 mg/mL in DSC buffer (25 mM Tris  
558 pH 8, 150 mM KCl, 1 mM TCEP, 10% glycerol). DSC measurements were performed on a

559 MicroCal Automated PEAQ-DSC instrument (Malvern Panalytical, Westborough, MA). Unless  
560 otherwise indicated, after a 5 min pre-scan equilibration step, samples were scanned from 10-  
561 120°C at a scan rate of 90°C/hr with no feedback. Data were analyzed using MicroCal PEAQ-  
562 DSC software, and baseline-subtracted data were fit to a non-two-state fitting model to obtain  
563 apparent  $T_m$  values.  
564

### 565 **Molecular Dynamics simulations**

566 Trajectories were run for 1.2  $\mu$ s - 3.7  $\mu$ s aggregate time for each complex. Starting  
567 conformations were taken from co-crystal structures of CaMKII $\alpha$  kinase domain in complex with  
568 peptides derived from GluN2B (PDB:6XBX) and Tiam1 (PDB:6XF0). For CaMKIIN1, Coot [41]  
569 was used to superimpose the structure of a peptide derived from rat CaMKIIN1 in complex with  
570 the kinase domain from *C. elegans* CaMKII (PDB:3KL8) with the structure of GluN2B in complex  
571 with the kinase domain of CaMKII $\alpha$  bound to a Mg<sup>2+</sup> ion and an ATP molecule (PDB:6XBX). The  
572 CaMKIIN1 peptide and the CaMKII $\alpha$  kinase domain were then merged into a single structure.  
573 Crystallographically unresolved atoms were added, peptides were extended in both N-terminal  
574 and C-terminal directions, and E236K mutant versions of GluN2B and Tiam1 systems were  
575 created using PDBFixer, part of the OpenMM package [42].  
576

577 All simulations were performed with Gromacs 2020.2 [43, 44] and the CHARMM36m force field  
578 [44]. Protein complexes were solvated with TIP3P water [45] in dodecahedral boxes that  
579 extended 1 nm past the protein in all dimensions. Na<sup>+</sup> ions were added in sufficient quantity to  
580 charge neutralize each system. Systems were energy-minimized by steepest descent for 50,000  
581 steps using a 0.01 nm step size until the maximum force exerted on any atom fell below 1000  
582 kJ/mol/nm. Solvent was equilibrated for 1 ns at constant temperature and volume (NVT  
583 ensemble) and another 2 ns at constant temperature and pressure (NPT ensemble) with a  
584 positional restraint applied to protein heavy atoms. Periodic boundary conditions were used in  
585 all dimensions, bonds were constrained with the LINCS algorithm [46], virtual sites (v-sites)  
586 were used to remove the fastest degrees of freedom to facilitate a 4 fs time step [47], particle  
587 mesh Ewald (PME) was used to treat electrostatic interactions [48], the v-rescale thermostat  
588 [49] with a 0.1 ps coupling time constant was used to maintain the temperature at 300 K, and a  
589 cut-off distance of 1.2 nm for neighbor list, Coulomb interactions, and Van der Waals  
590 interactions was used throughout system preparation and production simulations. The  
591 Parrinello–Rahman barostat [50] with a 2 ps coupling time constant was used to maintain a  
592 pressure of 1 bar during NPT equilibration and production simulations. V-site parameters for  
593 ATP were determined using MkVsites [51].  
594

595 One production simulation was performed for each of the wild type kinase:GluN2B and wild type  
596 kinase:Tiam1 complexes, producing trajectories of 2.19  $\mu$ s and 2.05  $\mu$ s, respectively. Two  
597 independent simulations were performed for each of wild type kinase:CaMKIIN1 and E236K  
598 kinase:GluN2B complexes. The CaMKIIN1 trajectories were 0.46  $\mu$ s and 1.84  $\mu$ s in length, for  
599 an aggregate of 2.3  $\mu$ s. The GluN2B trajectories were 0.68  $\mu$ s and 0.57  $\mu$ s in length, for an  
600 aggregate of 1.25  $\mu$ s. Four independent simulations were performed for the E236K  
601 kinase:Tiam1 complex, producing trajectories of 1.66  $\mu$ s, 1.23  $\mu$ s, 1.02  $\mu$ s, and 0.77  $\mu$ s, for an  
602 aggregate of 4.68  $\mu$ s. Trajectories were analyzed using MDTraj [52].  
603

### 604 **Coupled kinase assays**

605 Kinase activity was monitored using a Synergy H1 microplate reader (Biotek) as previously  
606 described [20, 53]. The assay was conducted in 50 mM Tris, 150 mM KCl, 10 mM MgCl<sub>2</sub>, 2 mM  
607 ATP, 1 mM Phosphoenolpyruvate (Alfa Aesar), 0.2 mM Nicotinamide adenine dinucleotide  
608 (Sigma), 10 units/mL Pyruvate kinase (Sigma), 30 units/mL Lactate dehydrogenase (Millipore

609 Sigma), varying concentrations of Syntide-2 (Lifetein). The final CaMKII kinase domain  
610 concentration was 5 nM. 500 nM CaMKIIN2 protein or 8.14  $\mu$ M NMDAR(S1303D) peptide was  
611 preincubated with CaMKII kinase domain before adding to the reaction mix of corresponding  
612 experiments. The reactions were started by the addition of ATP to the reaction mix and the  
613 absorbance was measured at 340 nM at 30°C at 10 and 15 sec intervals for 10 minutes. The  
614 rate was obtained by calculating the maximum observed slope of each reaction. Data were fit  
615 using the Michaelis-Menten equation in GraphPad PRISM version 6.01.

616

### 617 Immunoprecipitation

618 HEK293T cell lysates were prepared in lysis buffer (50 mM Tris-HCl pH 7.5, 150 mM NaCl, 1%  
619 Triton X-100, 10% glycerol, 1 mM  $\text{Na}_3\text{VO}_4$ , 10 mM NaF, 1 mM  $\beta$ -glycerophosphate, 1 x  
620 phosphatase inhibitor cocktail (Nacalai, Kyoto, Japan), 1x complete tablet (Roche, Basel,  
621 Switzerland) and centrifuged at 14,000 rpm for 10 min at 4°C. The supernatant was subjected to  
622 immunoprecipitation using 20  $\mu$ L of the anti-Flag antibody-beads (Sigma) for 2-4 hours at 4°C.  
623 Beads were washed with 1 mL of lysis buffer for three times. Bound proteins were eluted with  
624 SDS-PAGE sample buffer and subjected to western blotting.

625

### 626 Data availability

627 Atomic structures have been deposited in the PDB, listed in the table below.

628

629 Table of PDB codes and descriptions.

630

6X5G	Inactive kinase in complex with Densin-180
6X5Q	Inactive kinase in complex with GluA1
6X8V	Inactive kinase in complex with Tiam1
6XF0	Inactive kinase in complex with Tiam1 and ATP
6XBP	Inactive kinase in complex with GluN2B and Hecameg
6XBX	Inactive kinase in complex with GluN2B and ATP
6XDL	Active kinase in complex with GluN2B
6XDU	Active kinase in complex with GluN2B and ADP
7KL0	Inactive kinase in complex with phosphomimetic GluN2B and Hecameg
7KL1	Inactive kinase in complex with phosphomimetic GluN2B and ATP
7KL4	Inactive kinase in complex with phosphomimetic GluN2B
6XOE	Inactive kinase in complex with phosphomimetic GluN2B and ATP
7KL2	Inactive kinase in complex with phosphomimetic GluN2B

631

### 632 ACKNOWLEDGMENTS

633 We thank Roger Colbran for helpful discussions. This work was supported by start-up funds  
634 from UMass Amherst (M.S.), SPIRITS 2019 of Kyoto University, Grant-in-Aid for Scientific  
635 Research 18H04733, and 18H05434 from the MEXT, Japan and HFSP Research Grant  
636 (RGP0020/2019) (Y.H.).

637

638 Conflict of interest: YH received research funds from Fujitsu Laboratories and Dwango.

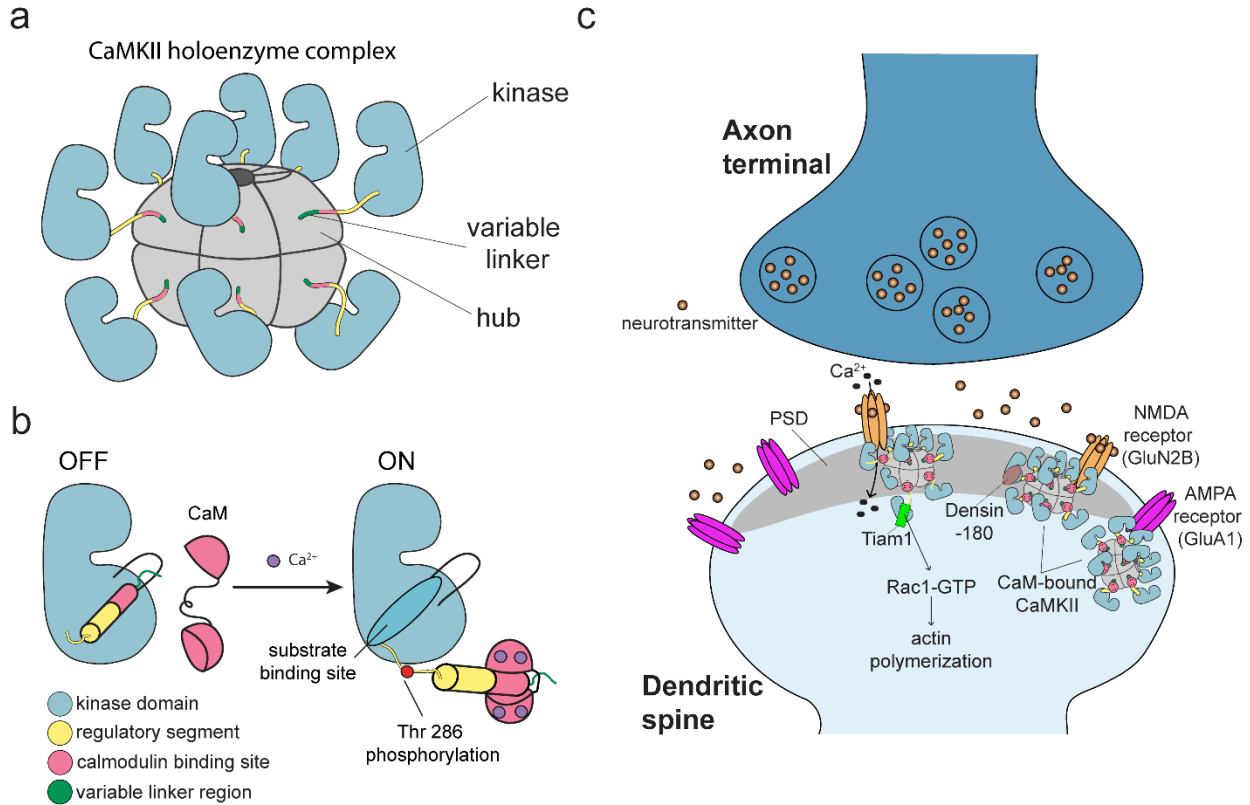
### 639 Author Contributions

640 C.Ö. solved all crystal structures and performed all FP measurements and kinetic assays. T.M.  
641 and T.S. performed immunoprecipitation experiments. N.S., E.A., C.G., E.L., J.F. and E.A.E.  
642 also assisted with experiments under supervision of B.A.K., S.C.G., Y.H. and M.M.S. R.S.

643 performed molecular dynamics. C.Ö., R.S., Y.H., B.A.K., and M.M.S. wrote and edited the  
644 manuscript.

645  
646

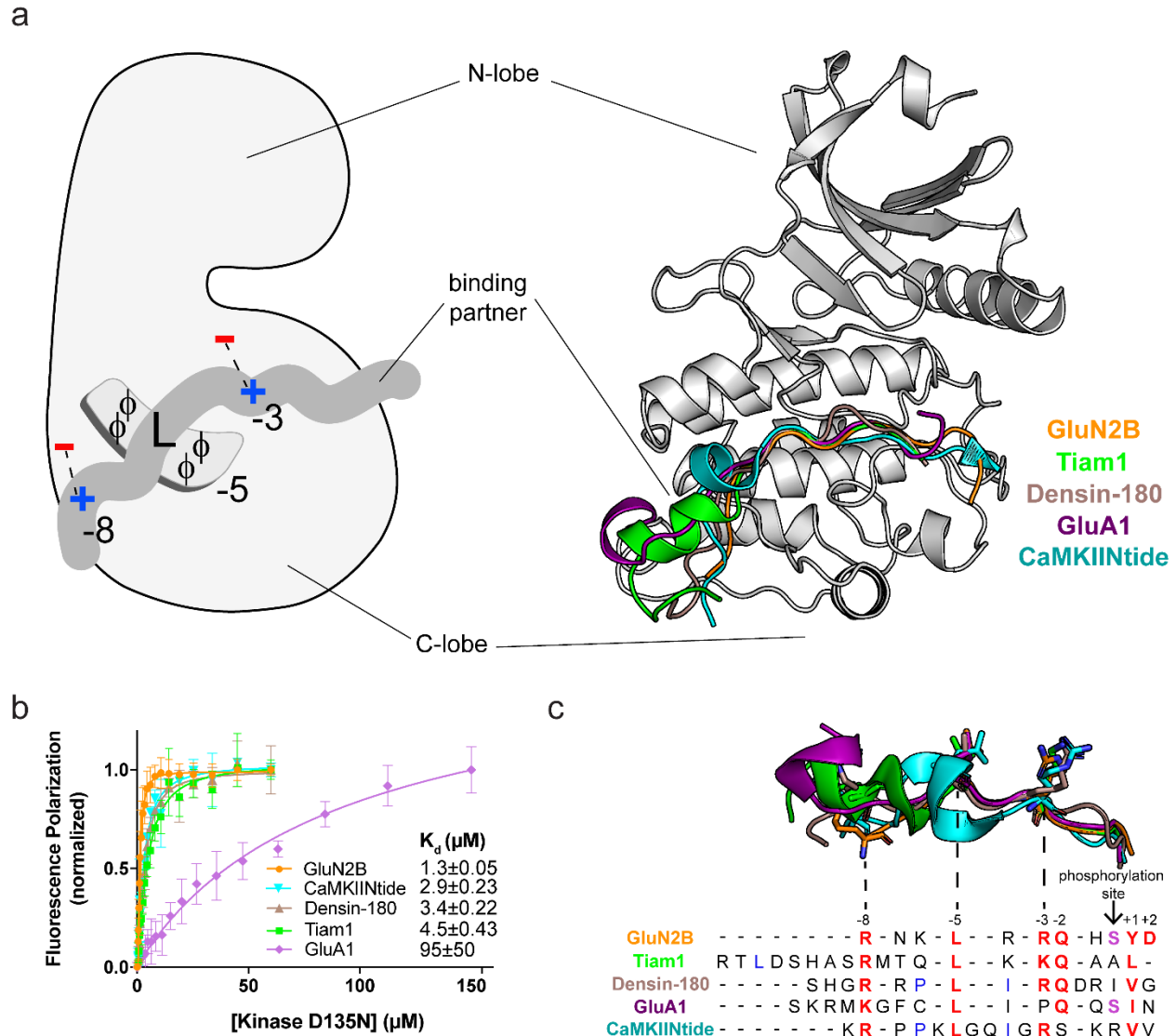
647 **FIGURES**



648  
649

650 **Figure 1. CaMKII architecture and the interaction partners at excitatory synapses**  
651 (a) The architecture of a dodecameric CaMKII holoenzyme. (b) Ca<sup>2+</sup>/CaM binding activates  
652 CaMKII by competitively binding the regulatory segment thereby freeing the substrate binding  
653 site. Active CaMKII autophosphorylates at Thr 286. (c) CaMKII interactions at the excitatory  
654 postsynaptic structure, mostly in the post synaptic density (PSD) of the dendritic spine.

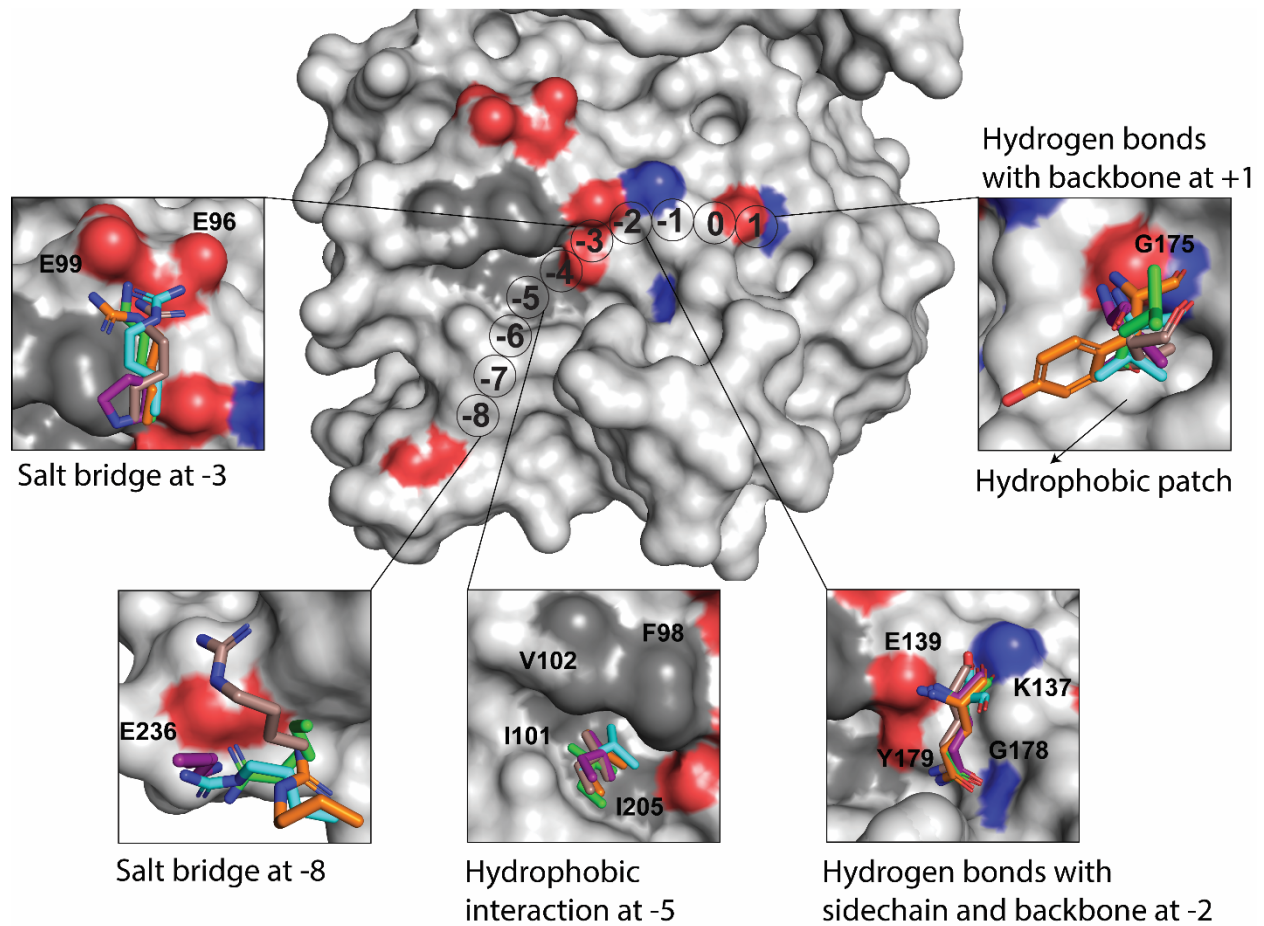
655  
656



657  
 658 **Figure 2. CaMKII kinase domain interactions with the binding partners.** (a) Left: Schematic  
 659 diagram of the interactions with binding partners. Phi symbol indicates hydrophobic residues.  
 660 Green symbols indicate those identified from molecular dynamics simulations. Right: overlay of  
 661 five cocrystal structures, peptides shown as cartoon in corresponding colors in (a). (b) Binding  
 662 measurements for GluN2B, Tiam1, Densin-180, CaMKIINtide, and GluA1 using fluorescence  
 663 polarization. (c) The sequence alignment of CaMKII binding partners. Aligned peptide structures  
 664 are above. Conserved residues highlighted in red. Phosphosite residues on substrates are  
 665 highlighted in purple. Residues involved in a docking event with W214 are highlighted in blue.  
 666



667



668

669

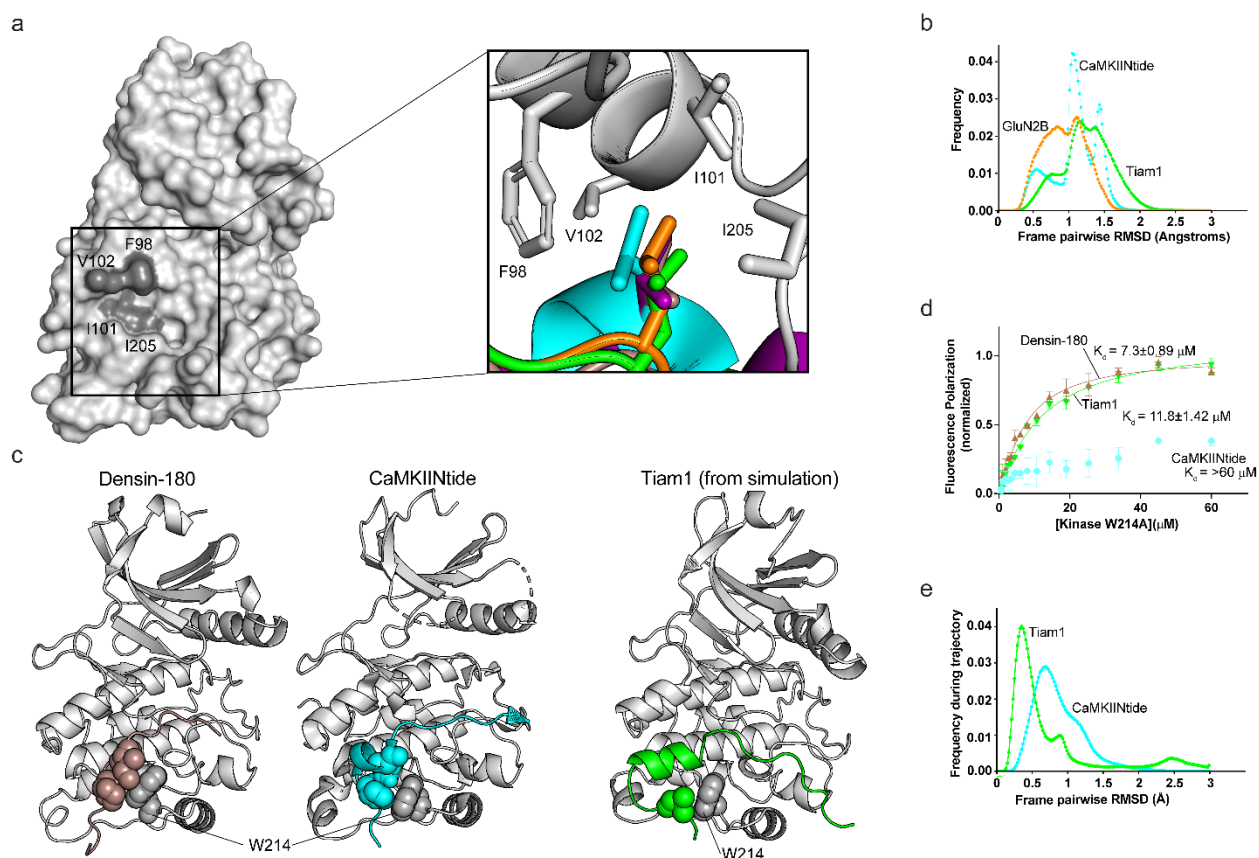
670

671

672

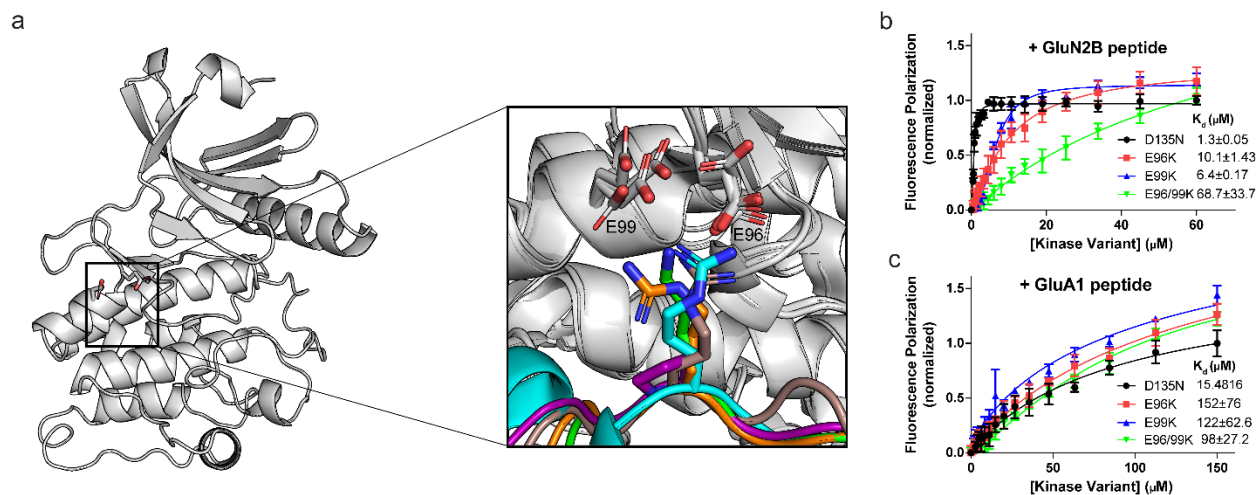
**Figure 3. Conserved binding motifs on the catalytic domain surface.**

Surface representation of the CaMKII kinase domain highlighting residues shown to interact with binding partners.



673  
 674 **Figure 4. Hydrophobic interactions mediate binding.** (a) Surface representation of CaMKII  
 675 kinase domain with residues forming the hydrophobic pocket labeled. Zoom in: Overlay of  
 676 leucine residues from all co-crystal structures bound in the hydrophobic pocket. (b) Histograms  
 677 of RMSD between every pair of trajectory frames for F98, I101, V102, and I205 with -5 peptide  
 678 leucine. (c) Sphere representation of the isoleucine and proline or leucine residue of Densin-180  
 679 (brown), CaMKIIN (cyan), and Tiam1 (green) docking onto W214 (gray) of kinase domain. (d)  
 680 FP measurements of the CaMKII kinase domain with W214A mutation binding to CaMKIIN  
 681 (cyan), Densin-180 (brown), and Tiam1 (green) peptides. (e) RMSD histograms for W214  
 682 interacting with isoleucine and proline of CaMKIIN1 and leucine of Tiam1 as seen in 3c.

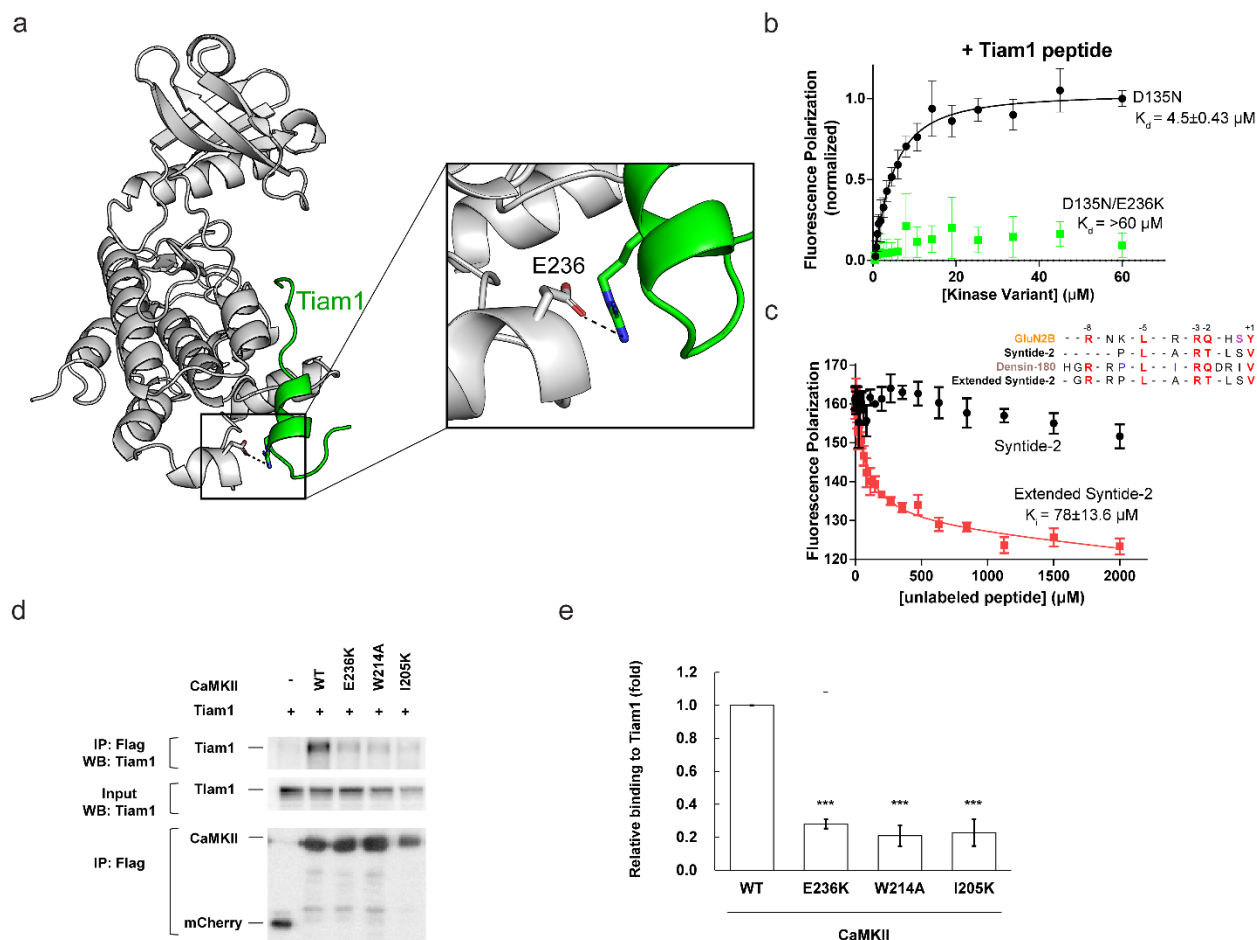
683  
 684  
 685



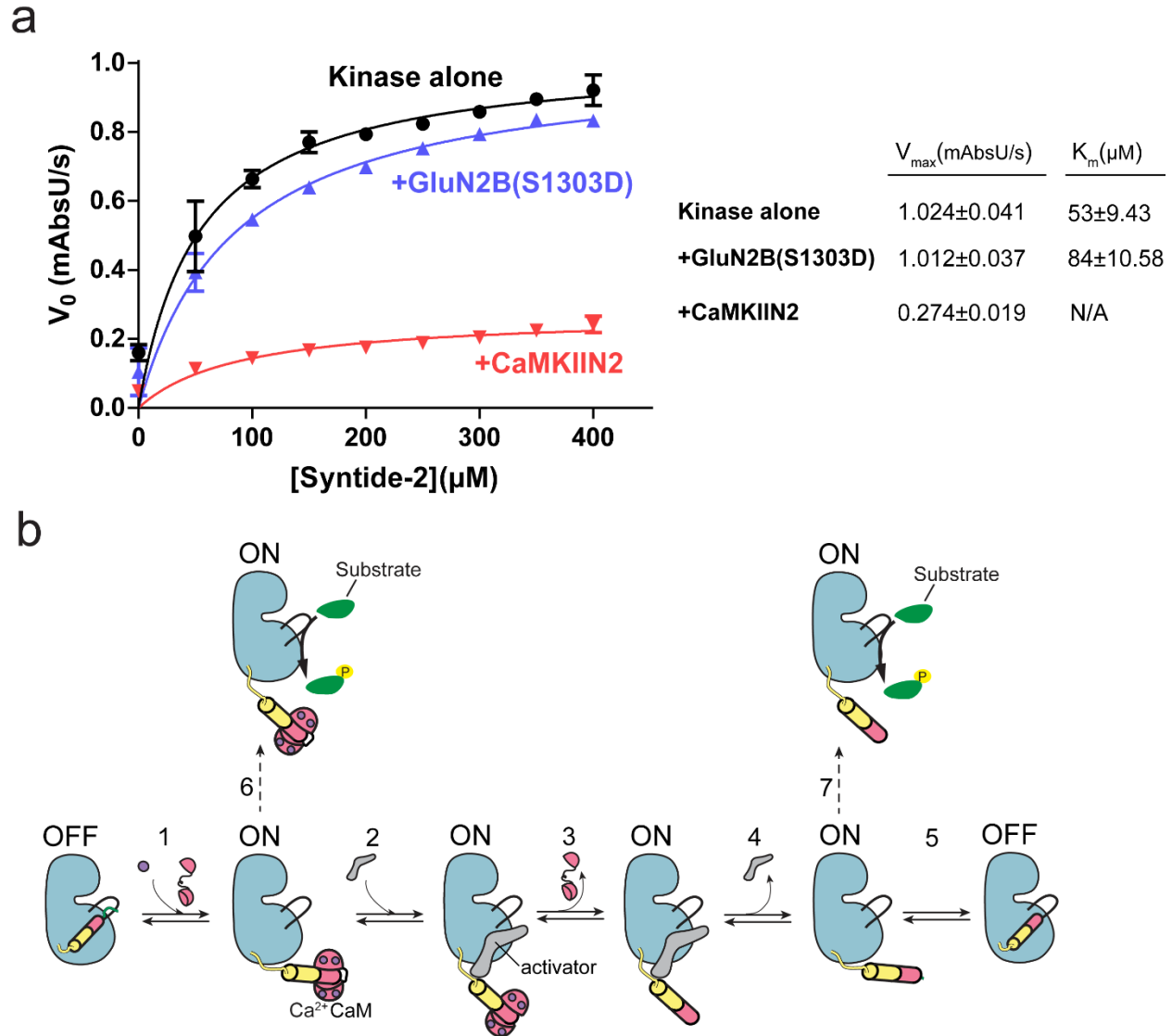
686  
687 **Figure 5. Electrostatic interactions with E6 and E9 facilitate high affinity binding.** (a)  
688 CaMKII kinase domain shown as a cartoon, E96 and E99 residues are shown in sticks. Inset:  
689 zoom in of all five co-crystal structures overlaid. (b) FP measurements of the CaMKII kinase  
690 domain with E96K (red), E99K (blue), and E9699K (green) mutations binding to the GluN2B  
691 peptide and (c) to the GluA1 peptide.

692  
693  
694  
695  
696  
697  
698

699



700  
 701 **Figure 6. Electrostatic interaction with E236 has distinctive effects on binding.** (a) View of  
 702 the interaction between CaMKII E236 residue (gray) and Tiam1 R1549 residue (green). (b) FP  
 703 measurements of the CaMKII kinase domain with E236K mutation binding Tiam1 (green)  
 704 peptide. (c) Competition assay against GluN2B using Syntide-2 (black) and extended version of  
 705 Syntide-2 (red). (d, e) Effects of CaMKII mutations (E236K, W214A and I205K) on interaction  
 706 with Tiam1. HEK293T cells were co-transfected with Flag-tagged CaMKII variants and Tiam1-  
 707 mGFP. Cell lysates were immunoprecipitated with Flag antibody, and samples were  
 708 immunoblotted with Tiam1 and Flag antibodies. (d) Representative blots. (e) Quantification of  
 709 the co-immunoprecipitated Tiam1 with CaMKII from 3 independent experiments. The amount of  
 710 co-immunoprecipitated Tiam1-mGFP was normalized by the amount in cell lysate and  
 711 immunoprecipitated CaMKII. \*\*\*p < 0.01, compared to WT CaMKII (n=3); one-way ANOVA with  
 712 the Shaffer's post hoc test comparisons. WT, wild type; IP, immunoprecipitation.  
 713



714  
715  
716  
717  
718  
719  
720  
721  
722  
723  
724  
725  
726  
727  
728  
729  
730  
731

**Figure 7. GluN2B acts as a competitive inhibitor on CaMKII** (a) Coupled kinase assay results with kinase alone, in the presence of GluN2B and CaMKIIN2. (b) Proposed model of maintaining CaMKII activity by binding to a high affinity activator. CaMKII binds  $Ca^{2+}/CaM$  and is activated (Rxn 1). Phosphorylation of substrates occurs in this state (Rxn 6). A high affinity activator binds to the substrate binding site (Rxn 2). When the  $Ca^{2+}$  signal dissipates, CaM dissociates from CaMKII, but the activator remains bound, competing with the regulatory segment (Rxn 3). The activator dissociates (Rxn 4), allowing another substrate to bind and be phosphorylated (Rxn 7) before either the regulatory segment rebinds (Rxn 5) or the activator rebinds (Rxn 4).

732 **Tables. Data Collection and Refinement Statistics**

733

734 **Table 1. GluN2B WT and S1303D cocrystal structures**

	GluN2B-ADP(Active Kinase) (6XU)	GluN2B(Active Kinase) (6XU)	GluN2B-ATP (6XK)	GluN2B-Hecameg (6XBP)	GluN2B(S1303D)-ATP (7KJ1)	GluN2B(S1303D)-ATP (8XQ1)	GluN2B(S1303D) (POB 7KL4)	GluN2B(S1303D) (POB 7KL2)	GluN2B(S1303D)+Hecameg (7KL0)
<b>Crystallization conditions</b>	0.1 M Bis-tris propane pH 6.5, 0.1 M Ammonium sulfate, 20% PEG 3350.	0.1 M Bis-tris propane pH 6.2, 0.1 M Ammonium sulfate, 20% PEG 3350, 5% Ethanol	0.1 M Bis-tris methane pH 6.2, 0.1 M Ammonium sulfate, 25% PEG 3350, 15mM Methyl 6-D-Heptylcarbamoyl-alpha-D-glucopyranoside	0.1 M Bis-tris methane pH 6.2, 0.1 M Ammonium sulfate, 25% PEG 3350, 15mM Methyl 6-D-Heptylcarbamoyl-alpha-D-glucopyranoside	0.1 M Bis-tris methane pH 6.5, 0.1 M Ammonium sulfate, 20% PEG 6000, 15mM Methyl 6-D-Heptylcarbamoyl-alpha-D-glucopyranoside	0.1 M Bis-tris propane pH 6.5, 0.2 M Sodium chloride, 25% PEG 3350	0.1 M Bis-tris propane pH 6.5, 0.2 M Sodium chloride, 25% PEG 3350	0.15 M DL-Malic acid pH 7, 20% PEG 3350	0.1 M Bis-tris methane pH 6.5, 0.1 M Ammonium sulfate, 20% PEG 6000, 15mM Methyl 6-D-Heptylcarbamoyl-alpha-D-glucopyranoside
<b>Data collection</b>									
<b>Space group</b>	P2 <sub>1</sub> 1	P2 <sub>1</sub> 1	P2 <sub>1</sub> 2 <sub>1</sub>	P2 <sub>1</sub> 2 <sub>1</sub>	P2 <sub>1</sub> 2 <sub>1</sub>	P2 <sub>1</sub> 1	P2 <sub>1</sub> 1	P2 <sub>1</sub> 1	P2 <sub>1</sub> 2 <sub>1</sub>
<b>Cell dimensions</b>									
a, b, c (Å)	45.01, 65.23, 53.71	45.00, 66, 45	73.14, 91.42, 91.02	73.25, 91.78, 91.77	72.80, 92.13, 91.34	47.31, 67.25, 45.72	43.40, 71.42, 45.27	44.78, 65.16, 54.1	72.99, 91.29, 92.08
α, β, γ (°)	90, 95.26, 90	90, 97.61, 90	90, 90, 90	90, 90, 90	90, 90, 90	90, 94.43, 90	90, 97.48, 90	90, 95.8, 90	90, 90, 90
<b>Resolution (Å)</b>	50 – 2.75 (2.85 – 2.8)	50 – 1.95 (1.99 – 1.96)	50 – 2.56 (2.60 – 2.56)	50 – 2.25 (2.29 – 2.25)	50 – 2.4 (2.44 – 2.4)	50 – 2.1 (2.14 – 2.1)	50 – 2.24 (2.28 – 2.25)	50 – 2.55 (2.59 – 2.55)	50-2.4 (2.44-2.4)
<i>R</i> <sub>meq</sub>	0.102 (0.374)	0.13 (0.485)	0.232 (0.812)	0.116 (0.374)	0.183 (0.527)	0.098 (0.297)	0.198 (1.671)	0.199 (0.778)	0.188 (0.627)
Mean I/σI	5 (1.57)	9.5 (2)	5 (1.80)	9.3 (4.36)	5.9 (2.65)	9.9 (3.51)	4.2 (0.524)	3.2 (0.44)	4.9 (2.04)
<b>Completeness (%)</b>	93.8 (90.9)	93.8 (82.7)	100 (99.8)	96.9 (96.1)	99.9 (98.8)	99.6 (97.3)	91.5 (75.5)	90.5 (97.7)	99.9 (99.5)
<b>Redundancy</b>	2.6 (2.5)	2.7 (2.5)	6.3 (5.4)	6.3 (5.7)	5.7 (5)	3.3 (2.8)	3.3 (2.8)	3.1 (2.6)	5.6 (4.9)
<b>CC<sub>1/2</sub></b>	0.985 (0.711)	0.956 (0.678)	0.976 (0.572)	0.98 (0.868)	0.976 (0.740)	0.943 (0.824)	0.979 (0.168)	0.975 (0.255)	0.984 (0.652)
<b>CC*</b>	0.996 (0.912)	0.888 (0.899)	0.994 (0.853)	0.997 (0.964)	0.994 (0.922)	0.948 (0.951)	0.995 (0.538)	0.994 (0.638)	0.996 (0.888)
<b>Refinement</b>									
<b>Resolution (Å)</b>	44.86 – 2.8 (2.824 – 2.753)	33.92 – 1.96 (2.002 – 1.951)	48.55 – 2.56 (2.626 – 2.56)	45.93 – 2.25 (2.31 – 2.252)	48.5 – 2.4 (2.46 – 2.4)	38.65 – 2.1 (2.154 – 2.1)	30.2 – 2.15 (2.296 – 2.25)	41.53 – 2.56 (2.623 – 2.56)	48.52 – 2.4 (2.46 – 2.4)
<b>Unique reflections</b>	7303 (428)	16929 (1027)	19465 (1411)	27648 (1847)	23497 (1650)	15852 (1096)	11903 (714)	9458 (577)	23396 (1610)
<i>R</i> <sub>meq</sub> / <i>R</i> <sub>int</sub>	17.9%/26.75%	18.41%/24.63%	20.33%/28.75%	18.83%/25.91%	19.01%/26.48%	17.82%/24.3%	21.87%/30.05%	24.17%/29.29%	19.17%/25.73%
<b>No. atoms</b>									
<b>Protein</b>	2235	2234	4479	4507	4518	2268	2243	2243	4497
<b>Water</b>	27	89	60	168	163	115	16	16	194
<b>Ligand</b>	31	35	82	64	108	44			94
<b>B-factors</b>									
<b>Protein</b>	39.05	31.23	32.11	38.04	28.16	28.73	49.80	49.80	26.25
<b>Water</b>	23.83	33.77	19.31	23.02	23.29	29.96	25.26	25.26	22.19
<b>Ligand</b>	74.28	45.19	50.76	76.47	34.43	41.75			34.51
<b>R.m.s. deviations</b>									
<b>Bond lengths (Å)</b>	0.0056	0.0085	0.0086	0.0083	0.0103	0.0081	0.0067	0.0049	0.0105
<b>Bond angles (°)</b>	1.4012	1.5357	1.6530	1.5758	1.6708	1.5531	1.4669	1.4676	1.7230

735

736 **Table 2. Tiam1, Densin-180 and GluA1 cocrystals structures**

	Tiam1-ATP (6XFO)	Tiam1 (6XRV)	Densin-180 (POB 6XSG)	GluA1 (6XSQ)
<b>Crystallization conditions</b>	16% PEG 6K, 0.1 M HEPES pH 7, 0.1% Triton X 114	0.1 M HEPES pH 7, 16% PEG 6K, 0.1% Triton X 114	0.1 M Bicine pH 5, 10% PEG 20K, 2% L4 Dioxane	0.1 M Tris pH 8, 28% PEG 4K
<b>Data collection</b>				
<b>Space group</b>	P2 <sub>1</sub> 2 <sub>1</sub> 1	P2 <sub>1</sub> 2 <sub>1</sub> 1	P2 <sub>1</sub> 1	P2 <sub>1</sub> 2 <sub>1</sub> 1
<b>Cell dimensions</b>				
a, b, c (Å)	43.49, 138.84, 154.97	43.43, 137.41, 156.47	36.29, 66.17, 61.71	42.63, 57.46, 107.71
α, β, γ (°)	90, 90, 90	90, 90, 90	90, 99.78, 90	90, 90, 90
<b>Resolution (Å)</b>	50 – 2.71 (2.76 – 2.71)	50 – 2.560 (2.6 – 2.56)	33.11 – 1.85 (1.88-1.85)	50 – 2.1 (2.18 – 2.14)
<i>R</i> <sub>meq</sub>	0.354 (2.294)	0.348 (2.359)	0.065 (0.325)	0.179 (0.377)
Mean I/σI	3 (0.5)	2.8 (0.42)	9.6 (3.14)	3.2 (2.23)
<b>Completeness (%)</b>	96 (89.7)	92.2 (90.9)	93.6 (86.5)	96.9 (92.7)
<b>Redundancy</b>	5.1 (3.8)	3.9 (2.8)	3.4 (3.3)	4.9 (4.4)
<b>CC<sub>1/2</sub></b>	0.975 (0.146)	0.962 (0.011)	0.99 (0.829)	0.992 (0.82)
<b>CC*</b>	0.994 (0.504)	0.99 (0.149)	0.997 (0.952)	0.998 (0.949)
<b>Refinement</b>				
<b>Resolution (Å)</b>	41.91 – 2.71 (2.783 – 2.713)	48.81 – 2.56 (2.622 – 2.56)	33.11 1.85 (1.88-1.85)	39.32 – 2.14 (2.159 – 2.104)
<b>Unique reflections</b>	23988 (1541)	27863 (1837)	22043 (3067)	34475 (798)
<i>R</i> <sub>meq</sub> / <i>R</i> <sub>int</sub>	22.86%/30.08%	26.03%/31%	18.65%/22.65%	18.93%/23.5%
<b>No. atoms</b>				
<b>Protein</b>	4461	4460	2250	2241
<b>Water</b>	83	30	111	96
<b>Ligand</b>	123	35	23	38
<b>B-factors</b>				
<b>Protein</b>	49.28	38.27	24.12	37.35
<b>Water</b>	24.5	11.57	25.6	24.48
<b>Ligand</b>	66.14	50.75	54.41	30.61
<b>R.m.s. deviations</b>				
<b>Bond lengths (Å)</b>	0.0077	0.0068	0.0095	0.0080
<b>Bond angles (°)</b>	1.5724	1.5884	1.6271	1.5184

737

738

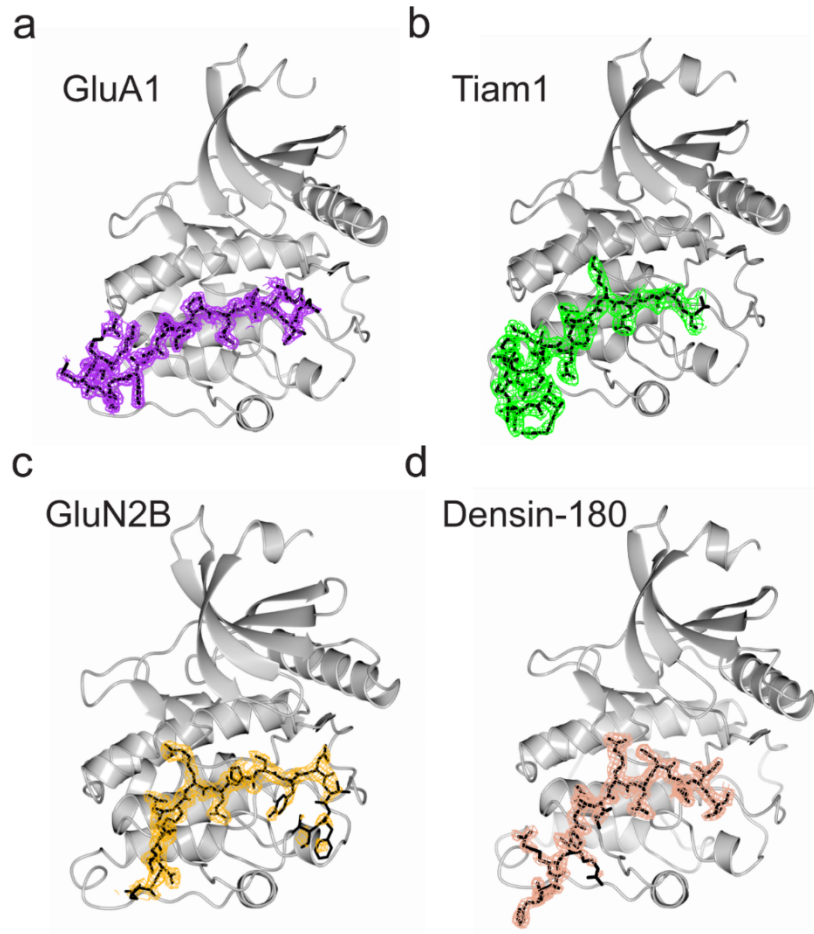
739

740

741

742

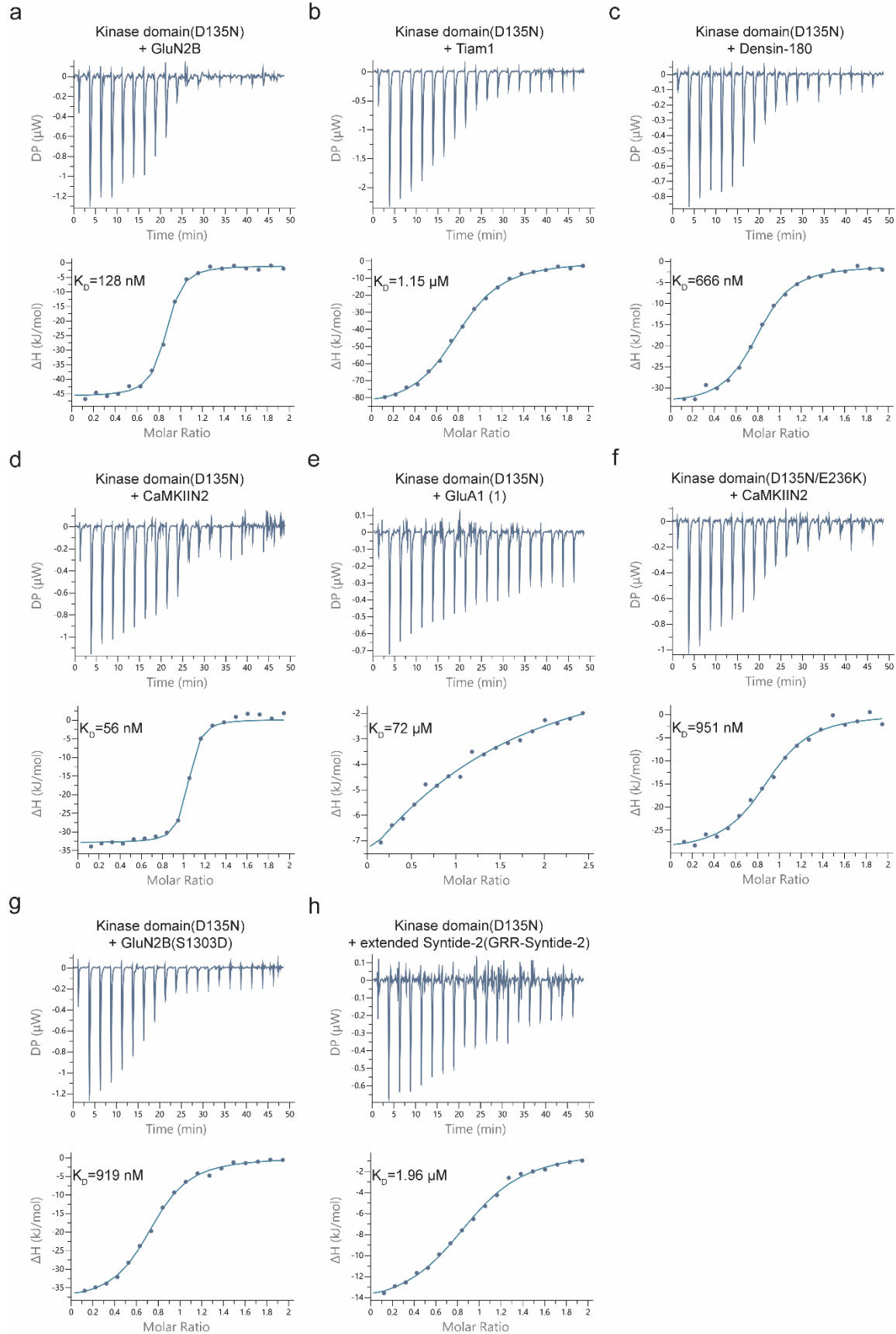
743 **SUPPLEMENTAL FIGURES**



744  
745  
746  
747  
748  
749

**Figure S1. Structures of CaMKII kinase domain bound to peptide binding partners.**

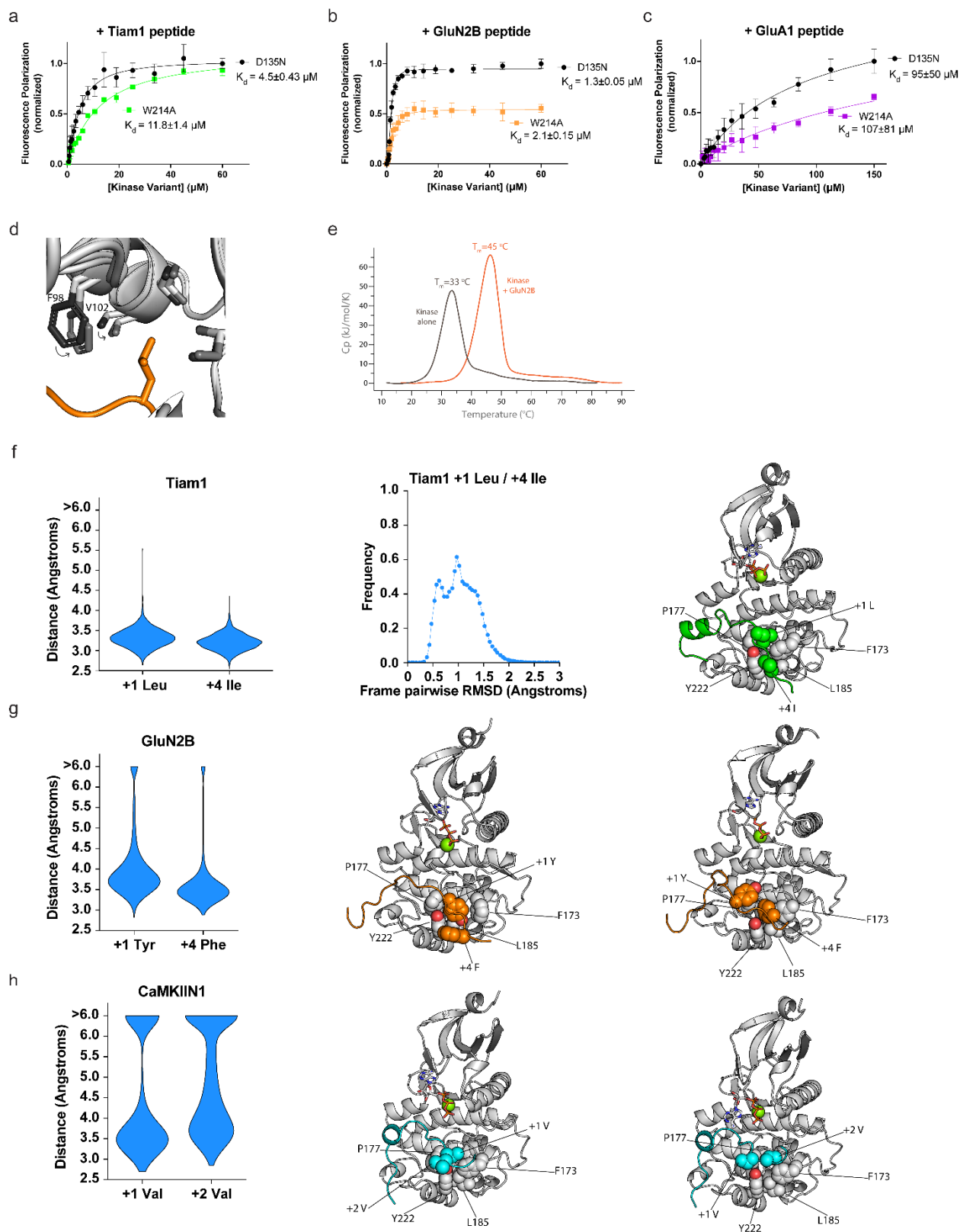
Electron density is shown for all peptide binding partners: (a) GluA1, (b) Tiam1, (c) GluN2B, and (d) Densin-180.



750



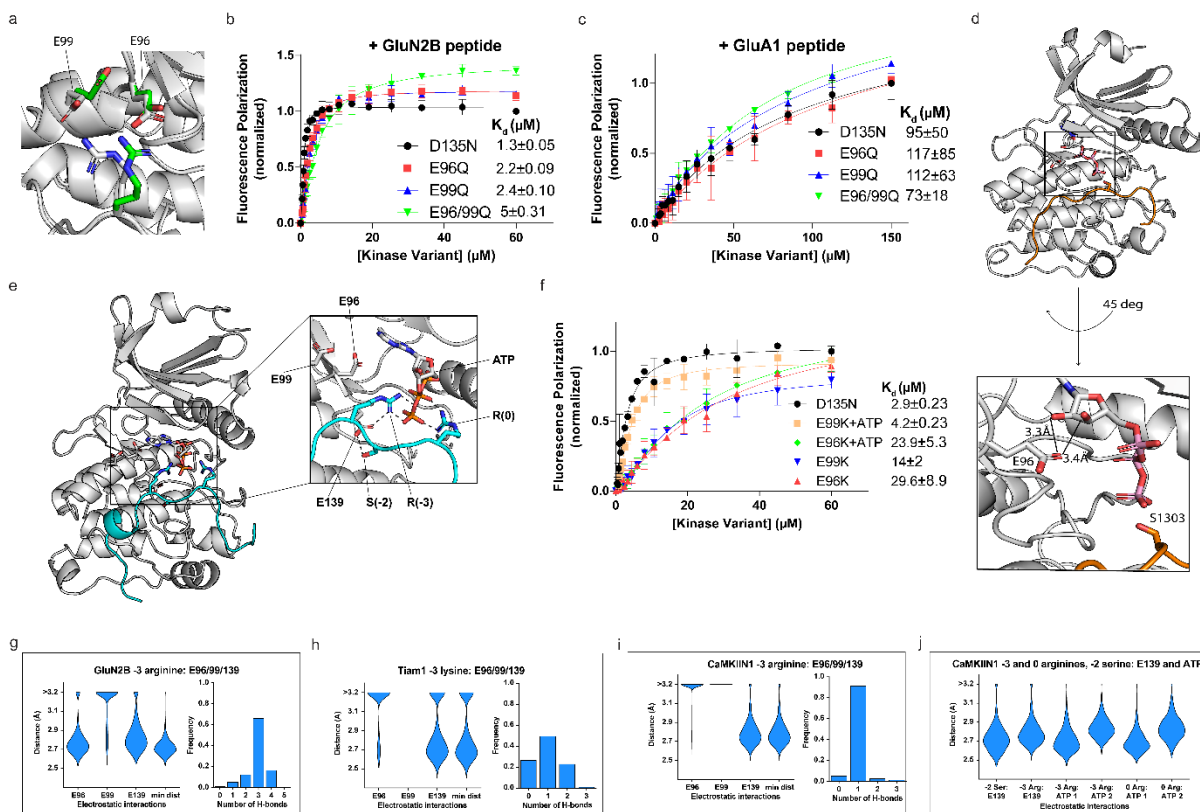
751 **Figure S2. ITC data show tighter binding to peptides in the absence of denaturant.**  
752 Isothermal scanning calorimetry data from CaMKII kinase domain (D135N) binding to (a)  
753 GluN2B peptide, (b) Tiam1 peptide, (c) Densin-180 peptide, (d) CaMKIIN2 protein, (e) GluA1  
754 peptide. (f) CaMKIIN2 protein with additional E236K mutation on the CaMKII kinase, (g) GluN2B  
755 (S1303D) peptide, and (h) extended Syntide-2 peptide.  
756



757  
758  
759  
760

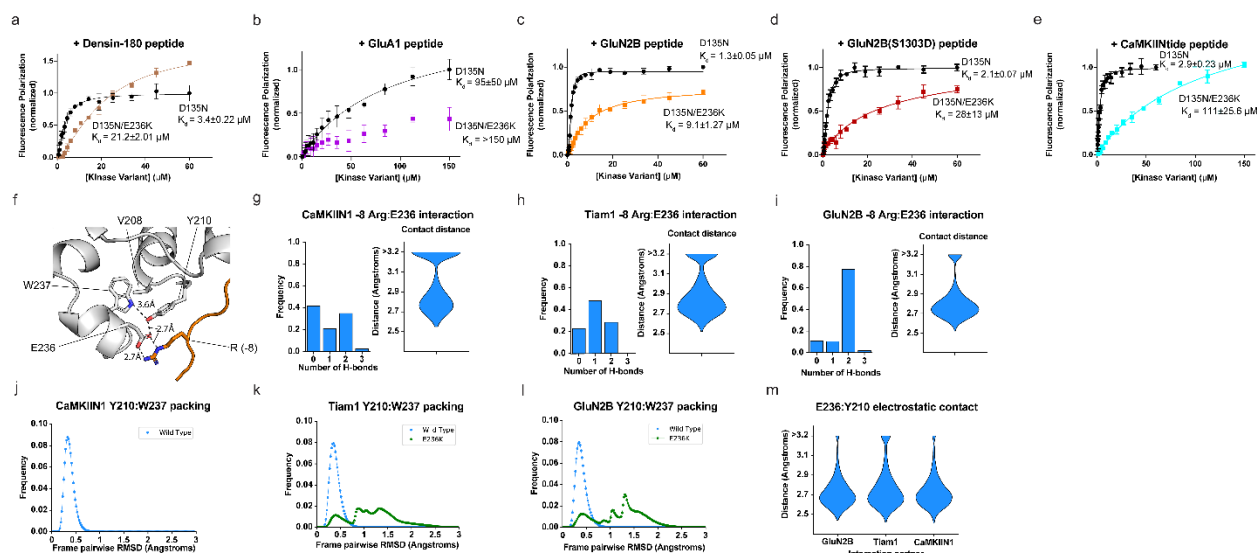
**Figure S3. Three hydrophobic interaction sites mediate peptide binding.** FP measurements of the CaMKII kinase domain with W214A mutation binding to (a) Tiam1 (green),

761 (b) GluN2B (orange), and (c) GluA1 (purple) peptides. (d) Overlay of CaMKII kinase domain  
 762 alone (PDB 6VZK) shown in dark gray and CaMKII kinase domain-GluN2B structure (PDB  
 763 6XBP) shown in lighter gray. F98 and V102 of CaMKII kinase domain undergo spatial  
 764 rearrangement upon leucine binding to the hydrophobic core. (e) Differential Scanning  
 765 Calorimetry data from CaMKII kinase domain alone (brown) and CaMKII kinase domain bound  
 766 to GluN2B peptide (orange). (f) Persistence of Tiam1 interaction with the F173, P177, L185,  
 767 Y222 hydrophobic patch in MD simulations. Distance distributions for +1 leucine and +4  
 768 isoleucine of Tiam1 to patch (left), RMSD histogram for +1 leucine, +4 isoleucine, and the four  
 769 residues that make up the patch (middle), representative structure (right). (g) Persistence of  
 770 GluN2B interaction with hydrophobic patch. Distance distributions for +1 tyrosine and +4  
 771 phenylalanine of GluN2B and two representative structures. (h) Persistence of CaMKIIN1  
 772 interaction with hydrophobic patch. Distance distributions for +1 and +2 valine residues of  
 773 CaMKIIN1 and two representative structures.  
 774



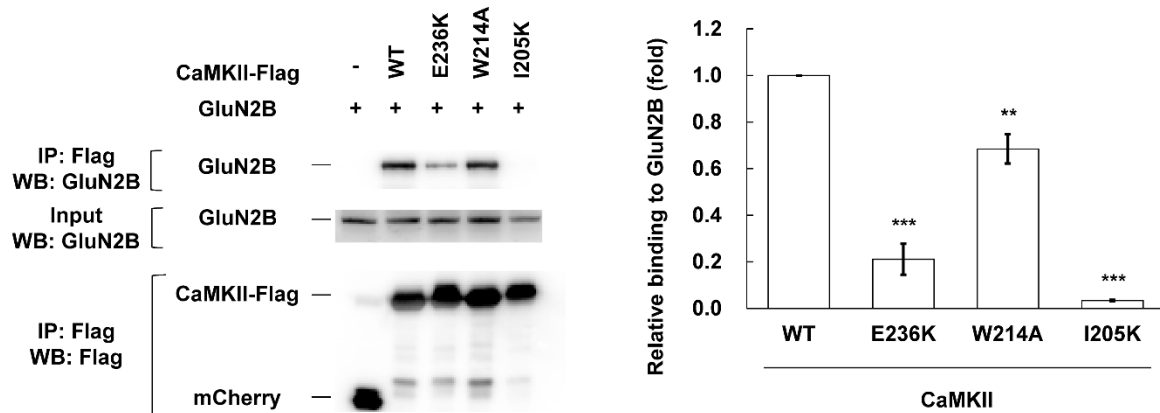
775  
 776  
 777 **Figure S4. E96, E99, and E139 regulate peptide interactions and ATP binding.** (a) R(-3) of  
 778 GluN2B peptide is seen in different orientations relative to E96 and E99 of CaMKII kinase  
 779 domain in separate crystal structures, 6XBP (light gray) and 6XDL (green). FP measurements of the  
 780 CaMKII kinase domain with E96Q-E99Q-E96/99Q mutations binding to GluN2B (b) and  
 781 GluA1 (c) peptides. (d) Co-crystal structure of CaMKII kinase domain and GluN2B in complex  
 782 with ATP (PDB 6XBX). Phosphorus shown in pink. Bottom image highlights the interaction  
 783 between E96 sidechain and ribose hydroxyl groups of ATP. (e) Snapshot from MD simulations  
 784 with CaMKIIN1 peptide in the presence of ATP. All interaction depicted with dashed lines are  
 785 below 3 Å. (f) FP measurements of CaMKII kinase domain with E96K-E99K mutations binding  
 786 to CaMKIIN1 in the absence and presence of ATP. (g-i) Electrostatic interactions between -3  
 787 peptide residue and E96, E99, and E139 in MD simulations. Distance distributions for -3 residue  
 788 to each glutamic acid side chain and shortest of the three distances (left) and histogram of the

789 number of H-bonds formed between the -3 residue and the three glutamic acid side chains  
 790 (right) for the (g) -3 arginine of GluN2b, (h) -3 lysine of Tiam1, and (i) -3 arginine of CaMKIIN1.  
 791 (j) Distance distributions for 0 arginine, -2 serine, and -3 arginine of CaMKIIN1 to E139 and and  
 792 to ATP phosphates. 0 and -3 arginines each make two contacts with ATP.  
 793

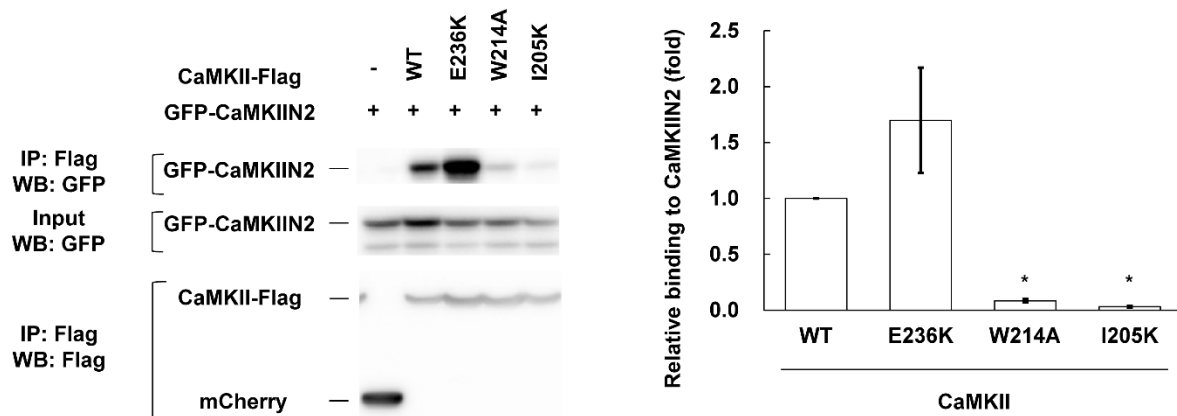


794  
 795  
 796 **Figure S5. E236 forms a large hydrogen bond network within the kinase domain.**  
 797 FP measurements of the CaMKII kinase domain with E236K mutation binding to (a) Densin-180  
 798 (brown), (b) GluA1 (purple), (c) GluN2B (orange), (d) GluN2B (S1303D) (red), (e) CaMKIINtide  
 799 (cyan) peptides. (f) Hydrogen bond network between W237, Y210, and E236 of CaMKII kinase  
 800 domain and R(-8) of GluN2B peptide. (g-i) Electrostatic interactions between R(-8) of peptide  
 801 and E236 in MD simulations. Histogram of the number of Hbonds (left) and distribution of  
 802 contact distance (right) for (g) CaMKIIN1, (h) Tiam1, and (i) GluN2B. (j-l) RMSD histograms for  
 803 hydrophobic packing of V208, Y210, and W237 in MD simulations of wild type kinase domain  
 804 (blue) and kinase domain with E236K mutation (green) for (j) CaMKIIN1, (k) Tiam1, and (l)  
 805 GluN2B. (m) Distance distributions for the electrostatic contact between E236 and Y210 in MD  
 806 simulations of wild type kinase domain with GluN2B, Tiam1, and CaMKIIN1.  
 807  
 808

a



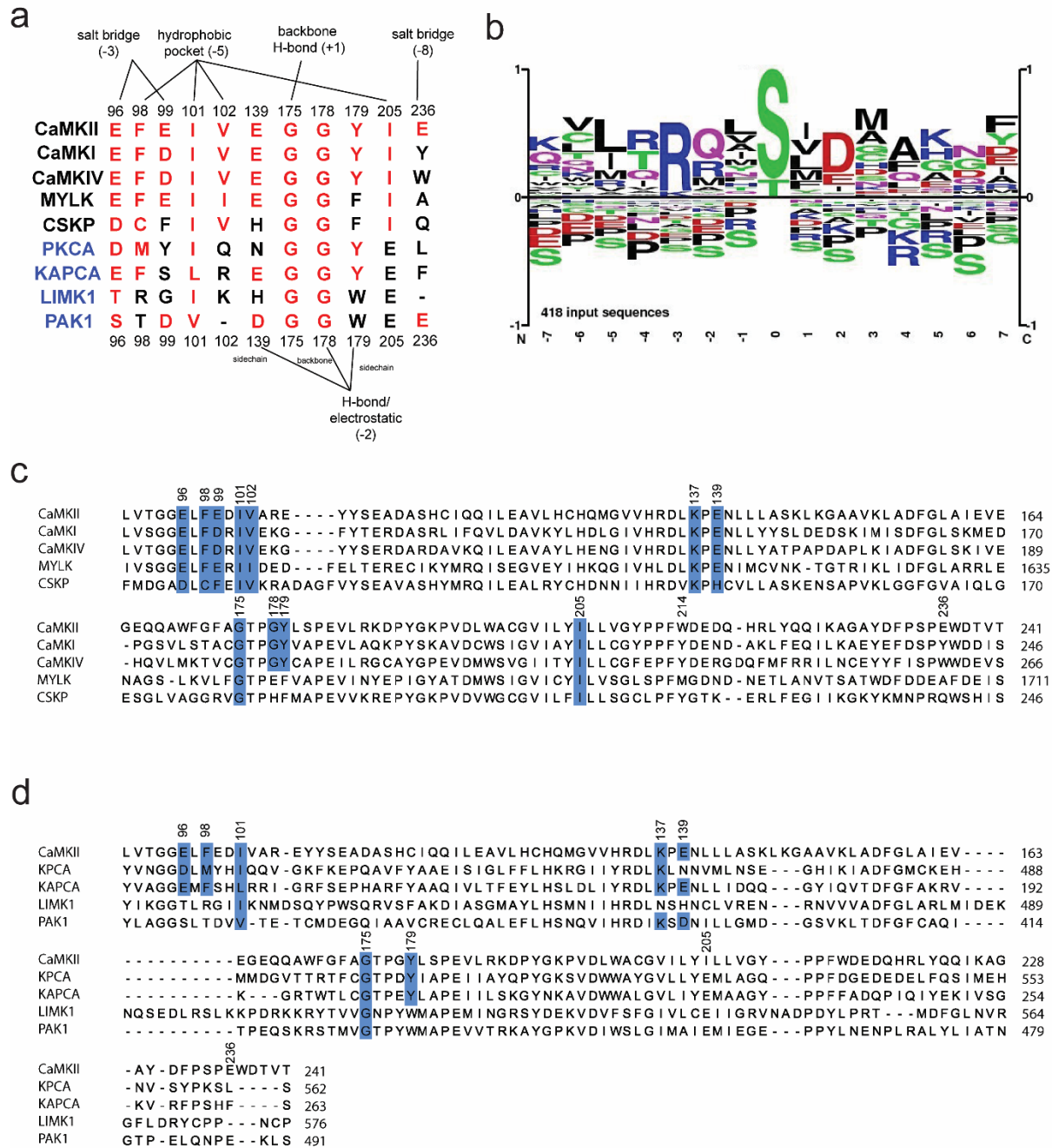
b



809  
810

811 **Figure S6. Effects of CaMKII mutations (E236K, W214A and I205K) on the interaction with**  
812 **full-length GluN2B and CaMKIIN2.**

813 HEK293T cells were co-transfected with Flag-tagged CaMKII and GluN2B or EGFP-CaMKIIN2.  
814 Cell lysates were immunoprecipitated with Flag antibody, and samples were immunoblotted with  
815 GluN2B, GFP and Flag antibodies. Representative blots were shown in (a) GluN2B, and (b)  
816 CaMKIIN2. The amount of co-immunoprecipitated GluN2B or CaMKIIN2 was normalized by the  
817 amount in cell lysate and immunoprecipitated CaMKII. Quantification of the co-  
818 immunoprecipitation from 3 or 4 independent experiments were shown in a graph of (a) GluN2B  
819 (n=3) (b) CaMKIIN2 (n=4). \*p < 0.05, \*\*, < 0.01 and \*\*\*, < 0.001, compared to WT CaMKII; one-  
820 way ANOVA with the Shaffer's post hoc test comparisons. WT, wild type; IP,  
821 immunoprecipitation.



822  
823  
824  
825  
826  
827  
828  
829  
830  
831

**Figure S7. Multi-sequence alignment of kinase domains.**

(a) Alignment of key residues involved in binding substrates across kinases from the Ca<sup>2+</sup>/CaM family (black text) and four kinases from different families (blue text). PKCA and KAPCA (cAMP dependent kinase) belong to the AGC Ser/Thr family. LimK1 and Pak1 belong to TKL and STE Ser/Thr family. (b) The sequence logo for all previously identified substrates of CaMKII from the PhosphoSitePlus database with the phosphorylation site at the 0 position. Conserved residues are highlighted blue. (c) across Ca<sup>2+</sup>/CaM family. (d) across different kinase families.

832  
833 **Supplementary Table 1. ITC values for CaMKII kinase domain binding to interaction**  
834 **partners**

In the cell	In the syringe	$K_D$ (nM)	N	$\Delta H$ (kJ/mol)	- $\Delta S$ (kJ/mol)	Cell/Syringe concentration ( $\mu M$ )
CaMKII KD (D135N)	GluN2B	128 $\pm$ 18.3	0.818 $\pm$ 5.5 x 10 <sup>-3</sup>	-44.9 $\pm$ 0.631	6.17	20/200
CaMKII KD (D135N)	Tiam1	1.15 x 10 <sup>3</sup> $\pm$ 90	0.795 $\pm$ 7.1 x 10 <sup>-3</sup>	-86.9 $\pm$ 1.5	53.5	20/200
CaMKII KD (D135N)	Densin-180	666 $\pm$ 91.1	0.779 $\pm$ 10 <sup>-2</sup>	-33.1 $\pm$ 0.803	-1.57	20/200
CaMKII KD (D135N)	CaMKIIN2	56.4 $\pm$ 12.5	0.992 $\pm$ 6.4 x 10 <sup>-3</sup>	-33 $\pm$ 0.384	-7.68	20/200
CaMKII KD (D135N)	GluA1	72 x 10 <sup>3</sup> $\pm$ 5.93 x 10 <sup>3</sup>	1	-20.4 $\pm$ 0.889	-2.82	40/500
CaMKII KD (D135N/E236K)	CaMKIIN2	951 $\pm$ 160	0.881 $\pm$ 1.8 x 10 <sup>-2</sup>	-29.8 $\pm$ 0.815	-4.07	20/200
CaMKII KD (D135N)	GluN2B (S1303D)	919 $\pm$ 100	0.725 $\pm$ 8.6 x 10 <sup>-3</sup>	-39 $\pm$ 0.864	5.11	20/200
CaMKII KD (D135N)	Extended Syntide-2 (GRR-Syntide-2)	1.91 x 10 <sup>3</sup> $\pm$ 273	0.908 $\pm$ 1.8 x 10 <sup>-2</sup>	-15.1 $\pm$ 0.581	-17	20/200

835  
836  
837 **REFERENCES**  
838

- 839 1. Lisman, J., R. Yasuda, and S. Raghavachari, *Mechanisms of CaMKII action in long-term*  
840 *potentiation*. Nat Rev Neurosci, 2012. **13**(3): p. 169-82.  
841 2. Malenka, R.C., et al., *An essential role for postsynaptic calmodulin and protein kinase*  
842 *activity in long-term potentiation*. Nature, 1989. **340**(6234): p. 554-7.  
843 3. Sloutsky, R. and M.M. Stratton, *Functional implications of CaMKII alternative splicing*.  
844 Eur J Neurosci, 2020.  
845 4. Erondy, N.E. and M.B. Kennedy, *Regional distribution of type II Ca<sup>2+</sup>/calmodulin-*  
846 *dependent protein kinase in rat brain*. J Neurosci, 1985. **5**(12): p. 3270-7.

- 847 5. Lynch, M.A., *Long-term potentiation and memory*. *Physiol Rev*, 2004. **84**(1): p. 87-136.
- 848 6. Ishida, A. and H. Fujisawa, *Stabilization of Calmodulin-Dependent Protein-Kinase-II*
- 849 *through the Autoinhibitory Domain*. *Journal of Biological Chemistry*, 1995. **270**(5): p.
- 850 2163-2170.
- 851 7. Bayer, K.U., et al., *Interaction with the NMDA receptor locks CaMKII in an active*
- 852 *conformation*. *Nature*, 2001. **411**(6839): p. 801-5.
- 853 8. Bayer, K.U., et al., *Transition from reversible to persistent binding of CaMKII to*
- 854 *postsynaptic sites and NR2B*. *J Neurosci*, 2006. **26**(4): p. 1164-74.
- 855 9. Saneyoshi, T., et al., *Reciprocal Activation within a Kinase-Effector Complex Underlying*
- 856 *Persistence of Structural LTP*. *Neuron*, 2019. **102**(6): p. 1199-1210 e6.
- 857 10. Strack, S. and R.J. Colbran, *Autophosphorylation-dependent targeting of calcium/*
- 858 *calmodulin-dependent protein kinase II by the NR2B subunit of the N-methyl- D-*
- 859 *aspartate receptor*. *J Biol Chem*, 1998. **273**(33): p. 20689-92.
- 860 11. Strack, S., R.B. McNeill, and R.J. Colbran, *Mechanism and regulation of*
- 861 *calcium/calmodulin-dependent protein kinase II targeting to the NR2B subunit of the N-*
- 862 *methyl-D-aspartate receptor*. *J Biol Chem*, 2000. **275**(31): p. 23798-806.
- 863 12. Omkumar, R.V., et al., *Identification of a phosphorylation site for*
- 864 *calcium/calmodulin-dependent protein kinase II in the NR2B subunit of the N-methyl-D-*
- 865 *aspartate receptor*. *J Biol Chem*, 1996. **271**(49): p. 31670-8.
- 866 13. Walikonis, R.S., et al., *Densin-180 forms a ternary complex with the (alpha)-subunit of*
- 867 *Ca<sup>2+</sup>/calmodulin-dependent protein kinase II and (alpha)-actinin*. *J Neurosci*, 2001.
- 868 **21**(2): p. 423-33.
- 869 14. Jiao, Y., et al., *Characterization of a central Ca<sup>2+</sup>/calmodulin-dependent protein kinase*
- 870 *IIalpha/beta binding domain in densin that selectively modulates glutamate receptor*
- 871 *subunit phosphorylation*. *J Biol Chem*, 2011. **286**(28): p. 24806-18.
- 872 15. Mammen, A.L., et al., *Phosphorylation of the alpha-amino-3-hydroxy-5-*
- 873 *methylisoxazole-4-propionic acid receptor GluR1 subunit by calcium/calmodulin-*
- 874 *dependent kinase II*. *J Biol Chem*, 1997. **272**(51): p. 32528-33.
- 875 16. Barria, A., V. Derkach, and T. Soderling, *Identification of the Ca<sup>2+</sup>/calmodulin-dependent*
- 876 *protein kinase II regulatory phosphorylation site in the alpha-amino-3-hydroxyl-5-*
- 877 *methyl-4-isoxazole-propionate-type glutamate receptor*. *J Biol Chem*, 1997. **272**(52): p.
- 878 32727-30.
- 879 17. Diering, G.H. and R.L. Huganir, *The AMPA Receptor Code of Synaptic Plasticity*. *Neuron*,
- 880 2018. **100**(2): p. 314-329.
- 881 18. Barria, A., et al., *Regulatory phosphorylation of AMPA-type glutamate receptors by CaM-*
- 882 *KII during long-term potentiation*. *Science*, 1997. **276**(5321): p. 2042-5.
- 883 19. Derkach, V., A. Barria, and T.R. Soderling, *Ca<sup>2+</sup>/calmodulin-kinase II enhances channel*
- 884 *conductance of alpha-amino-3-hydroxy-5-methyl-4-isoxazolepropionate type glutamate*
- 885 *receptors*. *Proc Natl Acad Sci U S A*, 1999. **96**(6): p. 3269-74.
- 886 20. Chao, L.H., et al., *Intersubunit capture of regulatory segments is a component of*
- 887 *cooperative CaMKII activation*. *Nat Struct Mol Biol*, 2010. **17**(3): p. 264-72.
- 888 21. Wang, C., et al., *A novel endogenous human CaMKII inhibitory protein suppresses tumor*
- 889 *growth by inducing cell cycle arrest via p27 stabilization*. *J Biol Chem*, 2008. **283**(17): p.
- 890 11565-74.



- 891 22. Zhang, J., et al., *Molecular cloning and characterization of a novel calcium/calmodulin-*  
892 *dependent protein kinase II inhibitor from human dendritic cells.* Biochem Biophys Res  
893 Commun, 2001. **285**(2): p. 229-34.
- 894 23. Chang, B.H., S. Mukherji, and T.R. Soderling, *Calcium/calmodulin-dependent protein*  
895 *kinase II inhibitor protein: localization of isoforms in rat brain.* Neuroscience, 2001.  
896 **102**(4): p. 767-77.
- 897 24. White, R.R., et al., *Definition of optimal substrate recognition motifs of Ca<sup>2+</sup>-calmodulin-*  
898 *dependent protein kinases IV and II reveals shared and distinctive features.* J Biol Chem,  
899 1998. **273**(6): p. 3166-72.
- 900 25. Songyang, Z., et al., *A structural basis for substrate specificities of protein Ser/Thr*  
901 *kinases: primary sequence preference of casein kinases I and II, NIMA, phosphorylase*  
902 *kinase, calmodulin-dependent kinase II, CDK5, and Erk1.* Mol Cell Biol, 1996. **16**(11): p.  
903 6486-93.
- 904 26. Ishida, A., et al., *Critical amino acid residues of AIP, a highly specific inhibitory peptide of*  
905 *calmodulin-dependent protein kinase II.* FEBS Lett, 1998. **427**(1): p. 115-8.
- 906 27. Stokoe, D., et al., *The substrate specificity and structure of mitogen-activated protein*  
907 *(MAP) kinase-activated protein kinase-2.* Biochem J, 1993. **296 ( Pt 3)**: p. 843-9.
- 908 28. Castro-Rodrigues, A.F., et al., *The Interaction between the Drosophila EAG Potassium*  
909 *Channel and the Protein Kinase CaMKII Involves an Extensive Interface at the Active Site*  
910 *of the Kinase.* J Mol Biol, 2018. **430**(24): p. 5029-5049.
- 911 29. Coultrap, S.J. and K.U. Bayer, *Improving a natural CaMKII inhibitor by random and*  
912 *rational design.* PLoS One, 2011. **6**(10): p. e25245.
- 913 30. Yang, E. and H. Schulman, *Structural examination of autoregulation of multifunctional*  
914 *calcium/calmodulin-dependent protein kinase II.* J Biol Chem, 1999. **274**(37): p. 26199-  
915 208.
- 916 31. Rellos, P., et al., *Structure of the CaMKII $\delta$ /calmodulin complex reveals the molecular*  
917 *mechanism of CaMKII kinase activation.* PLoS Biol, 2010. **8**(7): p. e1000426.
- 918 32. Rust, H.L. and P.R. Thompson, *Kinase consensus sequences: a breeding ground for*  
919 *crossstalk.* ACS Chem Biol, 2011. **6**(9): p. 881-92.
- 920 33. Zha, M., et al., *Crystal structures of human CaMKI $\alpha$  reveal insights into the*  
921 *regulation mechanism of CaMKI.* PLoS One, 2012. **7**(9): p. e44828.
- 922 34. Torres-Ocampo, A.P., et al., *Characterization of CaMKII  $\alpha$  holoenzyme stability.*  
923 Protein Science, 2020. **29**: p. 1524-1534.
- 924 35. Endicott, J.A., M.E. Noble, and L.N. Johnson, *The structural basis for control of eukaryotic*  
925 *protein kinases.* Annu Rev Biochem, 2012. **81**: p. 587-613.
- 926 36. Robison, A.J., et al., *Differential modulation of Ca<sup>2+</sup>/calmodulin-dependent protein*  
927 *kinase II activity by regulated interactions with N-methyl-D-aspartate receptor NR2B*  
928 *subunits and alpha-actinin.* J Biol Chem, 2005. **280**(47): p. 39316-23.
- 929 37. Mao, L.M., et al., *Phosphorylation and regulation of glutamate receptors by CaMKII.*  
930 Sheng Li Xue Bao, 2014. **66**(3): p. 365-72.
- 931 38. Hosokawa, T., et al., *Stoichiometry and phosphoisotypes of hippocampal AMPA-type*  
932 *glutamate receptor phosphorylation.* Neuron, 2015. **85**(1): p. 60-67.
- 933 39. McCoy, A.J., et al., *Phaser crystallographic software.* J Appl Crystallogr, 2007. **40**(Pt 4): p.  
934 658-674.

- 935 40. Murshudov, G.N., A.A. Vagin, and E.J. Dodson, *Refinement of macromolecular structures*  
936 *by the maximum-likelihood method*. Acta Crystallogr D Biol Crystallogr, 1997. **53**(Pt 3): p.  
937 240-55.
- 938 41. Winn, M.D., et al., *Overview of the CCP4 suite and current developments*. Acta  
939 Crystallogr D Biol Crystallogr, 2011. **67**(Pt 4): p. 235-42.
- 940 42. Eastman, P., et al., *OpenMM 4: A Reusable, Extensible, Hardware Independent Library*  
941 *for High Performance Molecular Simulation*. J Chem Theory Comput, 2013. **9**(1): p. 461-  
942 469.
- 943 43. Pall, S., et al., *Tackling Exascale Software Challenges in Molecular Dynamics Simulations*  
944 *with GROMACS*. Solving Software Challenges for Exascale, 2015. **8759**: p. 3-27.
- 945 44. Huang, J., et al., *CHARMM36m: an improved force field for folded and intrinsically*  
946 *disordered proteins*. Nat Methods, 2017. **14**(1): p. 71-73.
- 947 45. Jorgensen, W.L., et al., *Comparison of Simple Potential Functions for Simulating Liquid*  
948 *Water*. Journal of Chemical Physics, 1983. **79**(2): p. 926-935.
- 949 46. Hess, B., *P-LINCS: A Parallel Linear Constraint Solver for Molecular Simulation*. J Chem  
950 Theory Comput, 2008. **4**(1): p. 116-22.
- 951 47. Feenstra, K.A., B. Hess, and H.J.C. Berendsen, *Improving efficiency of large time-scale*  
952 *molecular dynamics simulations of hydrogen-rich systems*. Journal of Computational  
953 Chemistry, 1999. **20**(8): p. 786-798.
- 954 48. Essmann, U., et al., *A Smooth Particle Mesh Ewald Method*. Journal of Chemical Physics,  
955 1995. **103**(19): p. 8577-8593.
- 956 49. Bussi, G., D. Donadio, and M. Parrinello, *Canonical sampling through velocity rescaling*. J  
957 Chem Phys, 2007. **126**(1): p. 014101.
- 958 50. Parrinello, M. and A. Rahman, *Polymorphic Transitions in Single-Crystals - a New*  
959 *Molecular-Dynamics Method*. Journal of Applied Physics, 1981. **52**(12): p. 7182-7190.
- 960 51. Larsson, P., R.C. Kneiszl, and E.G. Marklund, *MkVsites: A tool for creating GROMACS*  
961 *virtual sites parameters to increase performance in all-atom molecular dynamics*  
962 *simulations*. J Comput Chem, 2020. **41**(16): p. 1564-1569.
- 963 52. McGibbon, R.T., et al., *MDTraj: A Modern Open Library for the Analysis of Molecular*  
964 *Dynamics Trajectories*. Biophys J, 2015. **109**(8): p. 1528-32.
- 965 53. Barker, S.C., et al., *Characterization of pp60c-src tyrosine kinase activities using a*  
966 *continuous assay: autoactivation of the enzyme is an intermolecular*  
967 *autophosphorylation process*. Biochemistry, 1995. **34**(45): p. 14843-51.  
968